Article

Not peer-reviewed version

The Exometabolome of *Xylella fastidiosa* in Contact with *Paraburkholderia phytofirmans* Supernatant Reveals Changes in Nicotinamide, Amino Acids, Biotin, and Plant Hormones

Oseias R. Feitosa-Junior *, Andrea Lubbe, Suzanne M. Kosina, Joaquim Martins-Junior, Deibs Barbosa, Clelia Baccari, Paulo A. Zaini, Benjamin P. Bowen, Trent R. Northen, Steven E. Lindow, Aline Maria Da Silva *

Posted Date: 7 December 2023

doi: 10.20944/preprints202311.1985.v2

Keywords: Xylella fastidiosa; Paraburkholderia phytofirmans; metabolomics; phytopathogen; liquid chromatography mass-spectrometry; MAGI

Article

The Exometabolome of *Xylella fastidiosa* in Contact with *Paraburkholderia phytofirmans* Supernatant Reveals Changes in Nicotinamide, Amino Acids, Biotin, and Plant Hormones

Oseias R. Feitosa-Junior [1,3,5,‡,*], Andrea Lubbe [2,µ], Suzanne M. Kosina [2], Joaquim Martins-Junior [1,§], Deibs Barbosa [1,•], Clelia Baccari [5], Paulo A. Zaini [4], Benjamin P. Bowen [2,3], Trent R. Northen [2,3], Steven E. Lindow [5] and Aline M. da Silva [1]

[1] Department of Biochemistry, Institute of Chemistry, University of Sao Paulo, Sao Paulo, 05508-900, SP, Brazil;
[2] Environmental Genomics and Systems Biology Division, Lawrence Berkeley National Laboratory, Berkeley, 94720, CA, USA;
[3] The DOE Joint Genome Institute, Berkeley, 94720, CA, USA;
[4] Department of Plant Sciences, University of California, Davis, 95616, CA, USA;
[5] Department of Plant and Microbial Biology, University of California, Berkeley, 94720, CA, USA;
* Correspondence: oseiasjr@iq.usp.br
‡ Current address: Genetics, Biocenter, Ludwig-Maximilian University of Munich, Munich, 82152, Germany.
µ Current address: Brightseed, The Bioactives Company, San Francisco, 94080, CA, USA.
§ Current address: National Biorenewables Laboratory, National Center for Energy and Materials Research (CNPEN), Campinas, 13083-100, SP, Brazil.
• Current address: Faculty of Medicine, University of Sao Paulo, São Paulo, 01246-903, SP, Brazil.

Abstract: Microbial competition within plant tissues affects invading pathogens' fitness. Metabolomics is a great tool for studying their biochemical interactions by identifying accumulated metabolites. *Xylella fastidiosa*, a Gram-negative bacterium causing Pierce's disease (PD) in grapevines, secretes various virulence factors including cell wall degrading enzymes, adhesion proteins, and quorum sensing molecules. These factors, along with outer membrane vesicles, contribute to its pathogenicity. Previous studies demonstrated that co-inoculating *X. fastidiosa* with *Paraburkholderia phytofirmans* strain PsJN suppressed PD symptoms. Here, we further investigated the interaction between the phytopathogen and the endophyte by analyzing the exometabolome of wild-type *X. fastidiosa* and a diffusible signaling factor (DSF) mutant lacking quorum sensing, cultivated with 20% *P. phytofirmans* spent media. LC-MS and MAGI were used to detect and map metabolites to genomes revealing a total of 121 metabolites, of which 25 were further investigated. These metabolites potentially relate to host adaptation, virulence, and pathogenicity. Notably, this study presents the first comprehensive profile of *X. fastidiosa* in the presence of *P. phytofirmans* spent media. The results highlight that *P. phytofirmans* and the absence of a functional quorum sensing affect the ratios of glutamine to glutamate (Gln:Glu) in *X. fastidiosa*. Additionally, two compounds with plant metabolism and growth properties, 2-Aminoisobutyric acid and Gibberellic Acid, were downregulated when *X. fastidiosa* interacted with *P. phytofirmans*. These findings suggest that *P. phytofirmans*-mediated disease suppression involves modulation of the exometabolome of *X. fastidiosa*, impacting plant immunity.

Keywords: *Xylella fastidiosa*; *Paraburkholderia phytofirmans*; metabolomics, phytopathogen, liquid chromatography mass-spectrometry, MAGI

1. Introduction

Deciphering molecular aspects of the interaction between *Xylella fastidiosa* and its plant hosts can provide important clues about disease development [1]. One key aspect leading to disease is its ability to modulate colonization behavior in plants and in insect vector transmission through quorum sensing (QS) mechanisms [2,3]. For this *X. fastidiosa* uses a family of modified fatty acids known as diffusible signaling factors (DSFs) that control individual and collective behavior and expression of virulence factors [4]. Many aspects contribute to the complexity of the disease at different molecular levels. These include the bacterium's capacity to become systemic, its ability to evade detection by the host immune system, and the subsequent overreaction of the plant immune system, causing, among other effects, plant water deprivation [1,5–7].

Microorganisms, including symbiotic bacteria, have the capacity to influence their host behavior by regulating the synthesis of specific compounds, thus fulfilling the metabolic and protein requirements of their host organisms [8–10]. Nevertheless, niche competition among microorganisms – a naturally environmental occurrence –, such as a spatial

Preprints (www.preprints.org) | NOT PEER-REVIEWED | Posted: 7 December 2023 doi:10.20944/preprints202311.1985.v2

dispute between a pathogen and an endophyte, often alters the fitness dynamics within the host [11,12]. Nutrient competition, nutrient provision, toxin secretion, and competitor predation – which are some relational possibilities among microorganisms and their hosts – can be unveiled by metabolite level alteration assessed by metabolomics [10,13–16].

X. fastidiosa causes diseases in several plant hosts of economic importance to world agriculture, including grapevines, almonds, citrus, and more recently olive trees [1,6,17,18]. This bacterium colonizes exclusively the lumen of xylem vessels of its plant hosts and is transmitted by insect vectors like sharpshooters throughout the Americas and a spittlebug *Philaenus spumarius* in Europe [19–21]. *X. fastidiosa* produces biofilm and secretes several virulence factors such as cell wall degrading enzymes (CWDE), and lipases/esterases, among others [22–24]. *X. fastidiosa* does not have the Type 3 Secretion System (T3SS), which in most bacterial pathogens is responsible for the delivery of effectors/virulence factors inside host cells [25–27], thus reflecting the lifestyle of this phytopathogen that colonizes xylem vessels, consisted mostly tissue consists mostly of dead lignified cells [28].

Paraburkholderia phytofirmans strain PsJN [29], known as a grapevine endophyte, multiplies within grapevines, similar to *X. fastidiosa* [30,31]. Co-inoculation with *X. fastidiosa* results in a significant reduction of the phytopathogen population and disease symptoms as previously reported for other pathogens [32]. This effect involves priming innate disease resistance pathways in grapevines leading to reduced symptoms when infected with *X. fastidiosa* [33]. Recently, in a subsequent study, *P. phytofirmans* PsJN, when topically applied with a surfactant, effectively controlled Pierce's Disease (PD) in grapevines, demonstrating systemic protection against *Xylella fastidiosa* infection, although the extent of protection was spatially limited, with potential implications for this endophyte use as a biological control agent [34].

Exometabolomics (or footprint), i.e., analysis of secreted metabolites, is a very effective approach to track signatures of microorganisms, e.g., contamination signatures [35]. Integrating metabolomics and genomics helps to track the origins of major trends in metabolite levels in different species, but also while interacting with each other [36,37]. In this sense, the characterization of the exometabolome is a useful tool to further understand the responses of *X. fastidiosa* to its environment and/or interactions with other organisms. In addition, the analysis of the exometabolome has many analytical advantages over the analysis of intracellular compounds due to their lower turnover, higher stability, and, consequently, a greater reproducibility of the metabolic footprint [38,39].

Here, we show that *P. phytofirmans* spent media is capable of disturbing *X. fastidiosa* mature biofilm formation *in vitro*. Additionally, we demonstrate the changes in the *X. fastidiosa* exometabolome triggered by *P. phytofirmans* spent media, providing further insights into the effect on QS and disease development.

2. Materials and Methods

Maintenance and Cultivation of Bacteria

Bacterial strains used in this work are listed in Table 1:

Table 1. List of bacteria and strains used in this work.

Bacteria	Strain	Original Host	Origin	Reference
Xylella fastidiosa	Temecula1 *Wild Type* (WT)	*Vitis vinifera*	Temecula, California, EUA	[27, 40]
	Δ*rpfF*	-	-	[41]
Paraburkholderia phytofirmans	PsJN	*Allium cepa*	Ontario, Canada	[42, 43]

X. fastidiosa was grown in PD3 medium (2 g/L starch; soytone 2 g/L; tryptone 4 g/L; 1 g/L sodium citrate; succinate 1 g/L; 10 mg/L hemin chloride; $MgSO_4$.$7H_2O$ 1 g/L; KH_2PO_4 1 g/L; K_2HPO_4 1.5 g/L) for 7 days. The WT and Δ*rpfF* strains were maintained in a PD3-agar medium. For Δ*rpfF*, PD3-agar had kanamycin added to a final concentration of 50 µg/ml.

For culture in liquid medium, after 7 days of culture in PD3-agar bacteria were transferred to 100 mL of PD3 medium and maintained at 28 °C at 100 rpm for up to 7 days. Cultures were started with OD_{600nm} = 0.05.

P. phytofirmans PsJN was selected from a plate of King's B medium [44] containing rifampicin (KBR) at 100 µg/mL. Next, *P. phytofirmans* was transferred to 100 ml of PD3. *X. fastidiosa* and *P. phytofirmans* were grown at 28 °C and 100 rpm. Fresh culture was started from frozen stocks at –80 °C.

Preprints (www.preprints.org) | NOT PEER-REVIEWED | Posted: 7 December 2023 doi:10.20944/preprints202311.1985.v2

Alternatively, WT and Δ*rpfF* strains were grown in PD3 supplemented with 20% of *P. phytofirmans* spent media. *P. phytofirmans* PsJN grown for 1 day in PD3 medium was centrifugated at 4000 *g* for 30 min, 4 °C, the supernatant was collected, adjusted to pH 4, and subjected to vacuum filtration through a 0.22 μm membrane. The eluate was added to a regular PD3 medium to a final concentration of 20% and used for subsequent experiments.

X. fastidiosa Biofilm Measurement

An aliquot (500 μL) of the *P. phytofirmans* PsJN spent medium eluate was added to 2.5 ml of PD3 liquid culture and then used to grow WT *X. fastidiosa* for 7 days at 28°C and 200 rpm. After this period the biofilm formed was quantified by staining with the crystal violet method as previously described [45]. Briefly, the biofilm deposited at the air-medium interface of the Temecula1 strain was washed with distilled water, stained for 20 min with 0.1% crystal violet reagent, washed again with distilled water, and then taken up in acetone: ethanol (6:4). Quantification was performed by measuring the absorbance at 595 nm (Abs_{595nm}).

Analysis of Metabolites of the Supernatant of X. fastidiosa Cultures by Liquid Chromatography Coupled to Mass Spectrometry (LC-MS)

Samples (1 mL) of spent medium from cultures and sterile control medium were centrifuged in 1.5 mL microcentrifuge tubes at 1700 *g* for 5 min. Supernatants, containing extracellular metabolites, were lyophilized and then resuspended in LC-MS grade methanol (300 μL). Resuspended samples were centrifuged again to pellet salts. Supernatants were dried under vacuum (Savant SpeedVac Plus SC110A) and resuspended in 500 μL of LC-MS grade methanol containing a mixture of internal standards (25 μM of 13C-15N-L-phenylalanine, 2-Amino-3-bromo-5-methylbenzoic acid, 3,6-dihydroxy-4-methylpyridazine, d4-lysine, d5-Benzoic acid, and 9-anthracene carboxylic acid). The samples were filtered through a 0.22 μm microcentrifuge filtration device and transferred to 1.5 mL borosilicate glass vials (Agilent) for LC-MS analysis as previously described [63]. Extraction blanks (blank microcentrifuge tubes taken through the entire extraction procedure to check for contaminants introduced during sample preparation) were included in the analysis. A quality control mixture (a defined mixture of common metabolites) and injection blanks (pure methanol) were also analyzed at the beginning and ends of each run to ensure no drift in retention times or signal abundances and no signs of column fouling or metabolite carryover. For polar metabolite analysis, an Agilent 1290 LC system equipped with a ZIC-pHILIC column (150 mm × 1 mm, 3.5 μm 100 Å, Merck Sequant) was used for metabolite separation with the following LC conditions: solvent A, 5 mM ammonium acetate; solvent B, 9:1 acetonitrile:H_2O with 5 mM ammonium acetate; timetable: 0 min at 100% B, 1.5 min at 100% B, 21 min at 0% B, 27 min at 0% B, 33 min at 100% B, and 45 min at 100% B; 0.8 mL/min; column compartment temperature of 40 °C. Mass spectrometry analyses were performed using a 6550 quadrupole time-of-flight mass spectrometer. Mass Spectrometry data were collected in a mass range of 30-1200 m/z, drying gas rate of 11 L/min, and gas temperature of 290 °C. Nebulizer pressure was set at 30 psi and capillary voltage was 3500 V. Data were acquired in both positive (+) and negative (–) polarity. The extracted samples were obtained in triplicate for both biological and technical replicates. Additionally, three replicate samples from sterile control media and eleven samples from extraction blanks were processed under the same conditions. A total of 62 injections were performed, including 3-11 replicate injections.

LCMS Data Processing and Analysis

Mass Hunter qualitative analysis software (Agilent, Santa Clara, CA, USA) was used to inspect the raw data. Then, the raw data obtained were parsed using Python scripts within MetAtlas [46], which was used to extract out putative metabolite peaks using an in-house metabolite database containing m/z and retention time data [46,47]. Next, the LC-MS data were analyzed using a custom code in Perl. Each of the detected peaks was evaluated to assign a level of confidence in the identification of the compound. Compounds that were identified had a corresponding retention time and m/z for a pure standard using the same methods as above. Negative and positive polarity mode lists of compounds were retrieved and merged, and compounds present in the negative mode were given preference over the detection in positive polarity mode. In order to confirm the identity of a compound, we checked the RT difference (i.e., $_{abs}[RT_{standard} - RT_{\mu experiment}]$) and the ppm error mass (i.e., $[(_{abs}[m/z_{standard} - m/z_{\mu experiment}])/m/z_{standard}] \times 10^6$) (Supplementary Table S1). Compounds with RT difference ≤ 0.05 and ppm error mass ≤ 6 were considered with their identities confirmed (Supplementary Table 1) [48]. Compounds that did not pass one or both criteria (up to ppm error mass ≤ 15) were considered putative. Next, compound abundance was normalized by strains OD in each biological replicate (Supplementary Table 2).

Preprints (www.preprints.org) | NOT PEER-REVIEWED | Posted: 7 December 2023 doi:10.20944/preprints202311.1985.v2

For further comparisons among conditions, it was considered expressed in the supernatants the compound that satisfied the following criteria: [μi_{sample} - μi_{blank}] - [μi_{medium} - μi_{blank}] > 0. Where μ stands for "average of peak area value" and *i* stands for any detected compound. Finally, an ANOVA test was conducted to acknowledge variability across all conditions (Supplementary Table S2). Compounds with a p-value ≤ 0.05 were considered statistically significant. Pairwise comparison among conditions was performed and a *t*-test with a p-adjusted value ≤ 0.05 was calculated for each compound. Compounds with statistical significance between two conditions were considered differentially expressed metabolites (DEM) (Supplementary Table S3). Extracted ion chromatograms (EIC) were generated, one representative EIC of each extract or exometabolome was used for building a summary panel for each discussed compound and all the remaining EIC from all biological and technical replicates were made available in the supplementary material (Supplementary Figures S1–S3).

A Python library for the Venn diagram was used to highlight unique and shared compounds across the conditions tested. These were referred to as *Xf* (*X. fastidiosa* WT Temecula1), Δ*rpfF* (*X. fastidiosa* ΔrpfF), Xf^{sm} (*X. fastidiosa* Temecula1 WT cultivated in PD3 media supplemented with 20% *P. phytofirmans* spent media), Δ$rpfF^{sm}$ (*X. fastidiosa* Δ*rpfF* cultivated in PD3 media supplemented with 20% *P. phytofirmans* spent media), and *P. phytofirmans* PsJN (*Pp*). A matrix was built from three biological replicates of *Xf*, Xf^{sm}, Δ*rpfF*, Δ$rpfF^{sm}$, and *Pp*. This matrix was given as an input to a multivariate data analysis in a principal coordinate analysis (PCoA) [49], taking as a parameter the Euclidean distance between the samples. To compute this dataset, we used the Python library skbio, and the library emperor to build the PCoA plot. Permanova and permdisp statistical analysis were made with the PCoA input data using skbio modules permanova and permdisp, respectively, and the information was added later to the PCoA plot.

A heatmap based on clustering of the compounds across conditions was generated with the Python libraries matplotlib and seaborn. The expression values of all compounds in all conditions were normalized by a z-score. A color code and symbols were added to compound names to indicate identification level and statistical significance.

Integration of Metabolites and Gene Set for Functional Annotation of Exometabolomes

Whole genome annotation (in fasta format) from *Xylella fastidiosa* Temecula1 and *Paraburkholderia phytofirmans* PsJN together with a list of InChiKey identifiers from all the compounds assigned as expressed in previous steps were given as input for a container (docker) of MAGI v1.0 [50,51] for metabolite and gene integration. The output spreadsheets were filtered by metabolites expressed in each given condition. Next, all genes annotated by MAGI were retrieved and duplicates were filtered out. Each gene list representing an exometabolome was submitted to the software OmicsBox [52] for functional annotation using gene ontology. Enrichment analysis was performed, annotations with p-value adj ≤ 0.05 were collected and the values were $\log_2$ transformed and ranked. The top 5 under and over-enriched annotations from each condition were collected for comparison. Matplotlib and seaborn Python libraries were used to build a bar plot.

Bioinformatic Analysis

Expressed metabolites were compared in box plot and bar plot, coded by matplotlib and seaborn Python libraries. Pairwise significance comparison was performed by the Python library statannotations, *t*-test argument was used. When necessary precomputed p-adjusted values for pairwise comparison were annotated later (Supplementary Table S2).

Metabolic reactions of nicotinamide, nicotinate, and biotin were freely redrawn from annotated *X. fastidiosa* and *P. phytofirmans* Kegg pathways. Illustrations of gene operons were rebuilt based on the synteny presented in the browser IMG/DoE [53]. Mummer [54] was used for the global alignment of genomic sequences.

For the metabolome and transcriptome integration, a bubble plot was created using matplotlib and seaborn Python libraries. The metabolites' expression values were $2^{z\text{-score}}$ transformed in order to maximize the expression differences and keep all values positive.

Cooperative Metabolic Interactions between X. fastidiosa and P. phytofirmans

In order to analyze the potential ecological microbial interactions [55] between *X. fastidiosa* and *P. phytofirmans*, a reverse ecology analysis was applied to predict the ecological structure of this symbiotic relationship [56].

For defining microbe-microbe cooperative and competitive potential in a pairwise manner, a local and customized NetSeed version [57] was used (to include the metabolic complementarity index and effective metabolic overlap index) [58, 59]. The metabolic complementarity index between two species measures the ratio (range 0–1) of acquired

Preprints (www.preprints.org) | NOT PEER-REVIEWED | Posted: 7 December 2023 doi:10.20944/preprints202311.1985.v2

compounds in one species that are found in the metabolic network of the other species and are not used by it. The effective metabolic overlap index of two species is the fraction of compounds required by both species and is, therefore, a measure of potential nutritional competition [58] with values ranging from 0 (no competition) to 1 (high competition).

3. Results

P. phytofirmans Interacts with X. fastidiosa through its Exometabolome

In a prior study, Baccari and colleagues [33] demonstrated that direct contact between *X. fastidiosa* and *P. phytofirmans* was not necessary for reducing *X. fastidiosa* titer loads in xylem vessels. Here we explore the indirect interaction between *X. fastidiosa* and *P. phytofirmans*, including the QS-insensitive mutant Δ*rpfF*. Following initial trials (unpublished data), we established a specific condition for subsequent experiments. We used PD3 culture media supplemented with 20% *P. phytofirmans* PD3 spent media, which noticeably affected the *X. fastidiosa* phenotype. This impact was particularly evident in terms of biofilm intensity and deposition, as measured by the Crystal Violet assay (Figure 1A).

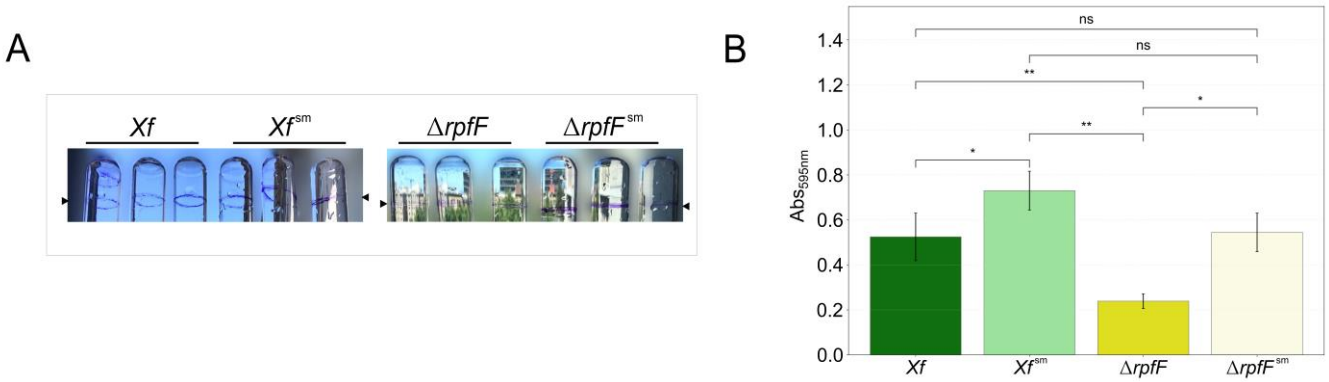

Figure 1. Biofilm increase in *X. fastidiosa* in response to exposure of *P. phytofirmans* secretome. **A.** Temecula1 WT or Δ*rpfF* strains were grown in PD3 medium for 7 days with (*Xf*^{sm} and Δ*rpfF*^{sm}) or without (*Xf* and Δ*rpfF*) 20% v/v of a 1-day PD3 medium *P. phytofirmans* (*Pp*) spent media. **A.** Glass tube image of the stained air-liquid interface of biofilm formation. **B.** Biofilm quantification was performed by measurement of crystal violet staining (Abs_{595nm}). Arrows indicate biofilm ring in the tubes. Error bars indicate the standard error of triplicate assays. Significantly different biofilm quantification was calculated using a *t*-test (ns: $p \leq 1.0\times10^{0}$, *: $1.0\times10^{-2} < p \leq 5.0\times10^{-2}$, **: $1.0\times10^{-3} < p \leq 1.0\times10^{-2}$).

During these experiments, we cultivated both *Xf* and Δ*rpfF* in regular PD3 culture media or supplemented with 20% *P. phytofirmans* PsJN spent media (*Xf*^{sm} or Δ*rpfF*^{sm}), and *Pp*. The biofilm formation of *Xf*^{sm} and Δ*rpfF*^{sm} increased by 39% and 128%, respectively (Figure 1B). Moreover, a larger amount of bacterial biomass was visually observed at the medium/air interface of *Xf*^{sm} and Δ*rpfF*^{sm} compared to *Xf* and Δ*rpfF* (Figure 1A). As PD3 supplemented with 20% *P. phytofirmans* spent media led to quantifiable changes in the biofilm formation profile of both bacterial strains in *in vitro* cultures, we hypothesized that the secreted metabolome (exometabolomes) of *P. phytofirmans* triggers a disturbance in the exometabolomes of the tested *Xylella* strains.

Exometabolome Variation among X. fastidiosa Strains in Response to P. phytofirmans

Subsequently, we investigated the exometabolomes of *Xf* and *Pp* to characterize the qualitative and quantitative signatures of compounds. By employing an internal reference library, we were able to identify a total of 131 compounds across all strains and experimental conditions (Supplementary Tables S1–S3). Referring to the detailed criteria for detection outlined in the Methods section, we established a threshold and inferred the detection of 121 compounds among the entire spectrum of strains and conditions examined (Supplementary Table S3) [48]. Specifically, within *Xf*, *Xf*^{sm}, Δ*rpfF*, Δ*rpfF*^{sm}, and *Pp*, we detected 114, 119, 118, 115, and 48 compounds, respectively (Figure 2A).

Preprints (www.preprints.org) | NOT PEER-REVIEWED | Posted: 7 December 2023 doi:10.20944/preprints202311.1985.v2

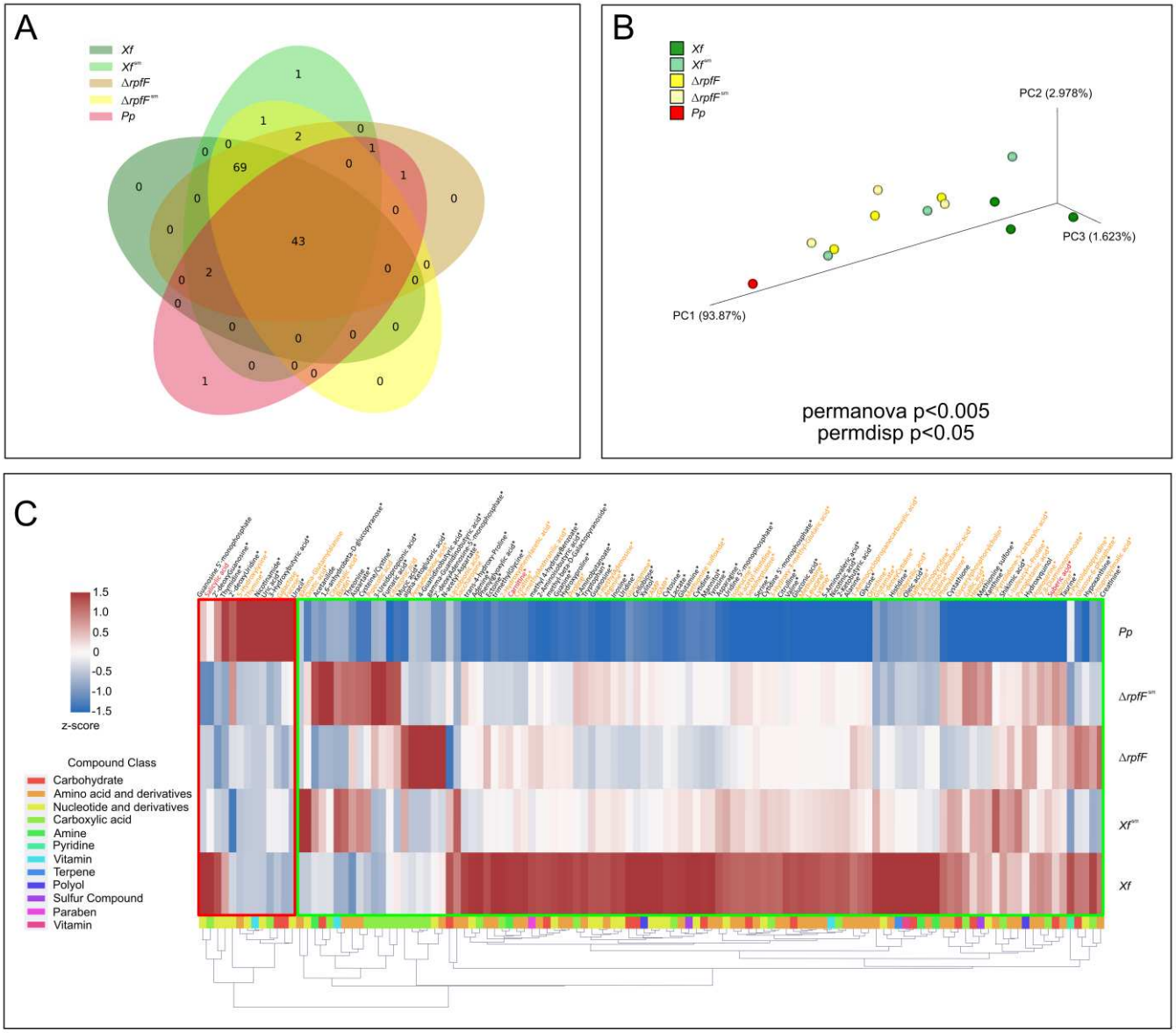

Figure 2. *X. fastidiosa* and *P. phytofirmans* exometabolomes. A. Venn Diagram of *Xf*, *Xf*^{sm}, Δ*rpfF*, Δ*rpfF*^{sm}, and *Pp* exometabolomes. Shared or exclusive metabolites detected in the *Xf*, *Xf*^{sm}, Δ*rpfF*, Δ*rpfF*^{sm}, and *Pp* exometabolomes are displayed. **B. Principal Coordinate Analysis (PCoA) of *Xf*, *Xf*^{sm}, Δ*rpfF*, Δ*rpfF*^{sm}, and *Pp* exometabolomes.** *Xf*, *Xf*^{sm}, Δ*rpfF*, Δ*rpfF*^{sm}, and *Pp* were cultured in PD3 medium for 7 days without (dark yellow and dark green circles) or with (light yellow and light green circles) 20% supernatant of *P. phytofirmans* PsJN; *Pp* was cultured in PD3 medium for 1 day (red circles). Each circle represents three technical replicates with 116 putative-identified metabolites. Permanova and Permidisp statistical analysis with 999 permutations were performed, the statistical significances are shown in the figure. **C. Heatmap representing the abundance of metabolites in the *Xf*, *Xf*^{sm}, Δ*rpfF*, Δ*rpfF*^{sm}, and *Pp* exometabolomes.** Each one of the 116 compounds detected in this study is indicated in the columns, each respective strain is indicated in the rows. The color code highlights the abundance of the metabolites in the conditions tested, ranging from low (blue), and medium (white) to high (red) expression. An additional column was added with the respective compound class as stated in PubChem. Two main clusters were highlighted, in green and red boxes, as they contain the compounds highly expressed in *X. fastidiosa* and *P. phytofirmans*, respectively. A z-score normalization was performed for each compound across the different conditions. Three biological replicates of each species and treatments were used for creating this heatmap. Compounds in black were confirmed by standard run comparison (regarding RT and m/z ppm), compounds in orange have a lower level of confirmation (either or both RT and m/z ppm), and compounds in red could not be confirmed by comparison RT. Low confidence compounds were

Preprints (www.preprints.org) | NOT PEER-REVIEWED | Posted: 7 December 2023 doi:10.20944/preprints202311.1985.v2

therefore considered as putative (possibly tautomer of the compound assigned). (*) indicates ANOVA statistical significance across conditions.

There is a shared core of 43 compounds present in all five exometabolomes. Focusing exclusively on the *X. fastidiosa* strains and treatments (*Xf*, *Xf*^{sm}, Δ*rpfF*, and Δ*rpfF*^{sm}), the Venn diagram highlights a core of 112 compounds. Notably, the Venn diagram also unveils a distinct subset of exclusive compounds (69) unique to *X. fastidiosa* (*Xf*, *Xf*^{sm}, Δ*rpfF*, and Δ*rpfF*^{sm}). The preeminent class of compounds within the core exometabolome belongs to "nucleotides and derivatives" (comprising 32.6% of the total). Among the exclusively expressed compounds found in *X. fastidiosa strains*, amino acids and derivatives dominate (52.2%). It is noteworthy that nicotinamide stands as the sole compound exclusively identified in *Pp* exometabolome, explored in further detail in the subsequent section.

Utilizing Principal Coordinate Analysis (PCoA), we discerned a distinct clustering pattern within the exometabolomes, initially delineating separation based on bacterial species (*Xf* versus *Pp*), and subsequently segregating according to strains and treatments (*Xf* versus Δ*rpfF*, and *Xf*^{sm} versus Δ*rpfF*^{sm}) (Figure 2B). This analysis yielded the formation of three primary and discernible clusters: (1) *Pp*, (2) *Xf*^{sm}, Δ*rpfF*, and Δ*rpfF*^{sm}, and (3) *Xf*. Notably, the implementation of Permanova and Permdisp analyses yielded statistically significant outcomes, denoted by p-values of <0.05 and <0.005, respectively, with respect to the distribution of samples.

Drawing from the outcomes of the PCoA, we postulate that the metabolites originating from *Pp* exert an influence on *Xf* exometabolomes, leading to a convergence in profile akin to that of the Δ*rpfF* metabolome. Interestingly, while Δ*rpfF* remains unaffected, as evidenced by the similarity to Δ*rpfF*^{sm} samples, this transformative effect is conspicuously absent. The PCoA not only highlights sample correlation but also offers a platform for constructing a working hypothesis. In essence, the assimilation of *Pp* spent media by *Xf* potentially results in a convergence of exometabolomic profiles, aligning *Xf* more closely with the characteristics of Δ*rpfF*, at least on the exometabolome level. A noteworthy observation is the similarity apparent in the sample distribution between Δ*rpfF* and Δ*rpfF*^{sm}. The distribution of exometabolome samples, as represented in Figure 2b, guides our hypothesis that the interaction of *Xf* with *Pp* spent media draws it near to the phenotype of Δ*rpfF*.

Finally, we generated a heatmap illustrating the expression levels of compounds, normalized by $2^{z\text{-score}}$. To enhance our comprehension of the functional attributes, variability, and expression levels of the metabolites, we organized the identified compounds into groups based on PubChem classes [60]. These groups correspond to various chemical classes, including carbohydrates, amino acids (and derivatives), nucleotides (and derivatives), carboxylic acids, pyridines, amines, sulfurs, terpenes, polyols, parabens, and vitamins. Noteworthy are the compounds that serve as intermediates within metabolic pathways and the citric acid cycle (such as α-ketoglutarate, fumarate, lactate, and succinate), along with secondary metabolites (including suberic acid and shikimic acid), present in the exometabolomes of both *X. fastidiosa* and *P. phytofirmans* (Figure 2C and Supplementary Table S3).

Within *Xf*, 75 metabolites demonstrated significantly upregulated expression levels compared to *Pp*, Δ*rpfF*, *Xf*^{sm}, and Δ*rpfF*^{sm}. Of these, 44% were amino acids and derivatives. Similarly, *Xf*^{sm} exhibited a majority of upregulated metabolites (5), accounting for 60% of amino acids and derivatives. Conversely, Δ*rpfF* and Δ*rpfF*^{sm} displayed 8 and 12 upregulated compounds, respectively, with 50% and 41,7% being carboxylic acids. In contrast, the *Pp* exometabolome exhibited notably low metabolite detection, particularly when contrasted with those identified in *Xf* exometabolomes. Of the detected metabolites in *Pp*, 10 exhibited upregulation when compared to their counterparts in *Xf* exometabolomes, of which 50% were nucleotides or nucleotide derivatives.

The heatmap construction encompassed all compounds detected above the threshold of blank (MeOH) and culture media (PD3 or PD3^{sm}), totaling 121 compounds. Our annotation approach included two additional layers of information—statistical significance, reflecting variance among conditions, and the level of identification. The heatmap (Figure 2C) encompasses compounds that met the criteria of standard confirmation through RT and m/z ppm, and annotations also included assigning compounds demonstrating statistical significance ($p < 0.05$) based on ANOVA analysis (Supplementary Tables 2 and 3). A notable feature of the heatmap is the emergence of two distinct clusters: one primarily composed of compounds highly expressed in *Pp*, and the other predominantly featuring compounds highly expressed in *Xf* strains. There exists a subset of compounds that are more highly expressed in *Xf*^{sm}, Δ*rpfF*, and Δ*rpfF*^{sm} in contrast to *Xf*. Upon a comprehensive review of the overall detected metabolites, we focused the investigation on a subset of 25 compounds (amino acids, vitamins, and plant hormones), as detailed in the subsequent sections.

 doi:10.20944/preprints202311.1985.v2

X. fastidiosa Secretes High Amounts of Amino Acids and Vitamins

First, we chose to further investigate compounds that are well known for their role in interaction between bacteria and some species of insect hosts [61]. For such, we examined amino acid levels among the strains and conditions.

The nutritional status of amino acids within the exometabolomes of *Xf*, Δ*rpfF*, *Xf*^{sm}, Δ*rpfF*^{sm}, and *Pp* was assessed, primarily utilizing the ratio of glutamine (GLN) to glutamate (GLU). This ratio, commonly employed to gauge nitrogen (N) status in various eukaryotic cells, has been linked to N limitation when <0.2 and indicative of N-replete cells when >0.5 [10,62]. The computed median GLN:GLU ratios within the exometabolomes unveiled variations: *Xf*, Δ*rpfF*, *Xf*^{sm}, and Δ*rpfF*^{sm} exometabolomes all exhibited ratios predicting N-replete conditions, spanning from 0.52:1 in *Xf* to 8.33:1 in Δ*rpfF* (Figure 3A). Notably, Gln and Glu were not detected within the exometabolome of *Pp* under the assessed conditions. The 0.5 threshold for N-replete conditions was drawn in the plot, with all conditions (*Xf*, *Xf*^{sm}, Δ*rpfF*, and Δ*rpfF*^{sm}) surpassing this threshold—except for *Pp*, which lies below, and *Xf*, which teeters at the threshold. Importantly, our analysis did not identify any statistically significant differences between *Xf*, *Xf*^{sm}, Δ*rpfF*, and Δ*rpfF*^{sm}.

Preprints (www.preprints.org) | NOT PEER-REVIEWED | Posted: 7 December 2023 doi:10.20944/preprints202311.1985.v2

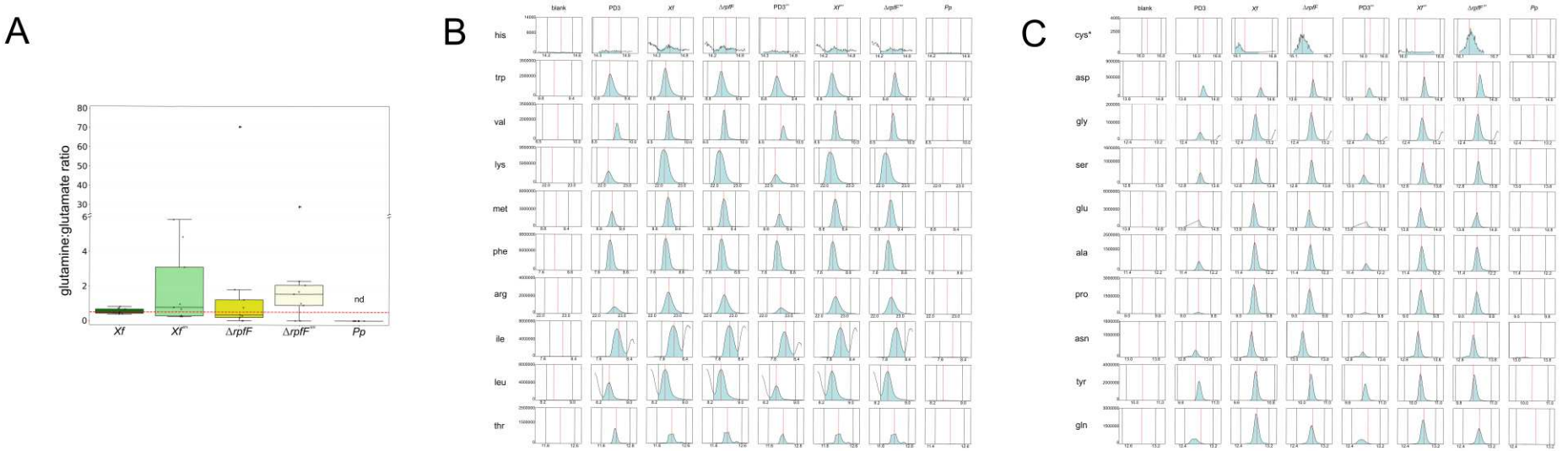

Figure 3. Nitrogen status of *Xf*, Δ*rpfF*, *Xf*^{sm}, Δ*rpfF*^{sm}, and *Pp* exometabolomes. A. glutamine:glutamate ratio. Average expression of Glutamine and Glutamate, from 3 biological replicates and 3 technical replicates, were used to calculate the gln:glu ratio. Dotted line indicates the "0.5", a ratio indicating cellular N-replete. **B.** EAA and **C.** nEAA EICs of representative assessments in blank (MeOH), PD3, PD3^{sm}, *Xf*, Δ*rpfF*, *Xf*^{sm}, Δ*rpfF*^{sm,} and *Pp* extracts or exometabolomes.

Preprints (www.preprints.org) | NOT PEER-REVIEWED | Posted: 7 December 2023 doi:10.20944/preprints202311.1985.v2

In order to provide a comprehensive understanding of compound levels within the experimental framework, we constructed a panel of EIC encompassing various controls, including the blank (MeOH), and culture media controls, PD3 and PD3^{sm} (Figures 3B,C; Supplementary Figures S1 A–T). These control conditions were juxtaposed with the investigated states: *Xf*, *Xf*^{sm}, Δ*rpfF*, Δ*rpfF*^{sm}, and *Pp*. As anticipated, control conditions (culture media PD3 and PD3^{sm}) exhibited detectable amino acid levels. Upon scrutinizing *Xf*, *Xf*^{sm}, Δ*rpfF*, and Δ*rpfF*^{sm}, a noticeable pattern emerges: amino acid levels, whether pertaining to nEAA or EAA, consistently surpass those found in the blank samples and even exceed the amino acid concentrations in the culture media controls. This observation aligns with the knowledge that PD3, given its protein-rich composition, inherently contains a source of amino acids. Upon closer examination, this elevated amino acid content within *Xf*, *Xf*^{sm}, Δ*rpfF*, and Δ*rpfF*^{sm} challenges conventional assumptions, indicating a plausible role as an insect-vector decoy within its presumed biological function. In stark contrast, the levels of EAA and nEAA in *Pp* are notably diminished, bordering on complete absence.

While the visual inspection of differences in the levels of essential amino acids (EAA) and non-essential amino acids (nEAA) does not consistently yield pronounced distinctions, we undertook individual assessments of these two amino acid categories. The nature of this evaluation displayed variability across species, strains, and treatments, with notable statistical significance emerging primarily between amino acid quantifications in *Xf* and *Xf*^{sm}. Specifically, variations were evident in tyrosine, serine, proline, glutamine, aspartate, asparagine, alanine, and glycine within the nEAA, and valine, methionine, lysine, leucine, isoleucine, and arginine within the EAA. Similarly, only histidine exhibited a discernible difference between Δ*rpfF* and Δ*rpfF*^{sm} (Figures 3B,C). Notably, within the exometabolome of *Pp*, neither EAA nor nEAA were detected.

Given the disparities in ionization among amino acids, merging them into a unified value for comparison across diverse conditions is not viable. Nonetheless, a consistent observation emerges: essential amino acids (EAA) exhibit higher individual abundance within *Xf*, *Xf*^{sm}, Δ*rpfF*, and Δ*rpfF*^{sm} in comparison to non-essential amino acids (nEAA).

We also investigated levels of complex B vitamin detected in the tested exometabolomes. These compounds are relevant to the relationship between insect and host plant. Our findings illustrate the accumulation of nicotinamide in *Pp*, while it is notably absent in *Xf*, *Xf*^{sm}, Δ*rpfF*, and Δ*rpfF*^{sm}—this absence is evident across both normalized values (peak area intensity by OD) and EIC profiles, including comparison with controls. Conversely, the presence of nicotinic acid follows an inverse pattern (Figure 4A–F, Supplementary Figure S2A–C). The product of *pncA*, namely nicotinic acid, exhibits high expression in *Xf*, along with downregulation and relatively consistent levels in *Xf*^{sm}, Δ*rpfF*, and Δ*rpfF*^{sm}. Biotin, on the other hand, was not detected in *Xf*, Δ*rpfF*, or *Pp*. In contrast, its presence was identified at relatively low levels in *Xf*^{sm} and Δ*rpfF*^{sm}. The pathways remain conserved in both *X. fastidiosa* and *P. phytofirmans* (Figure 4G,H).

Preprints (www.preprints.org) | NOT PEER-REVIEWED | Posted: 7 December 2023 doi:10.20944/preprints202311.1985.v2

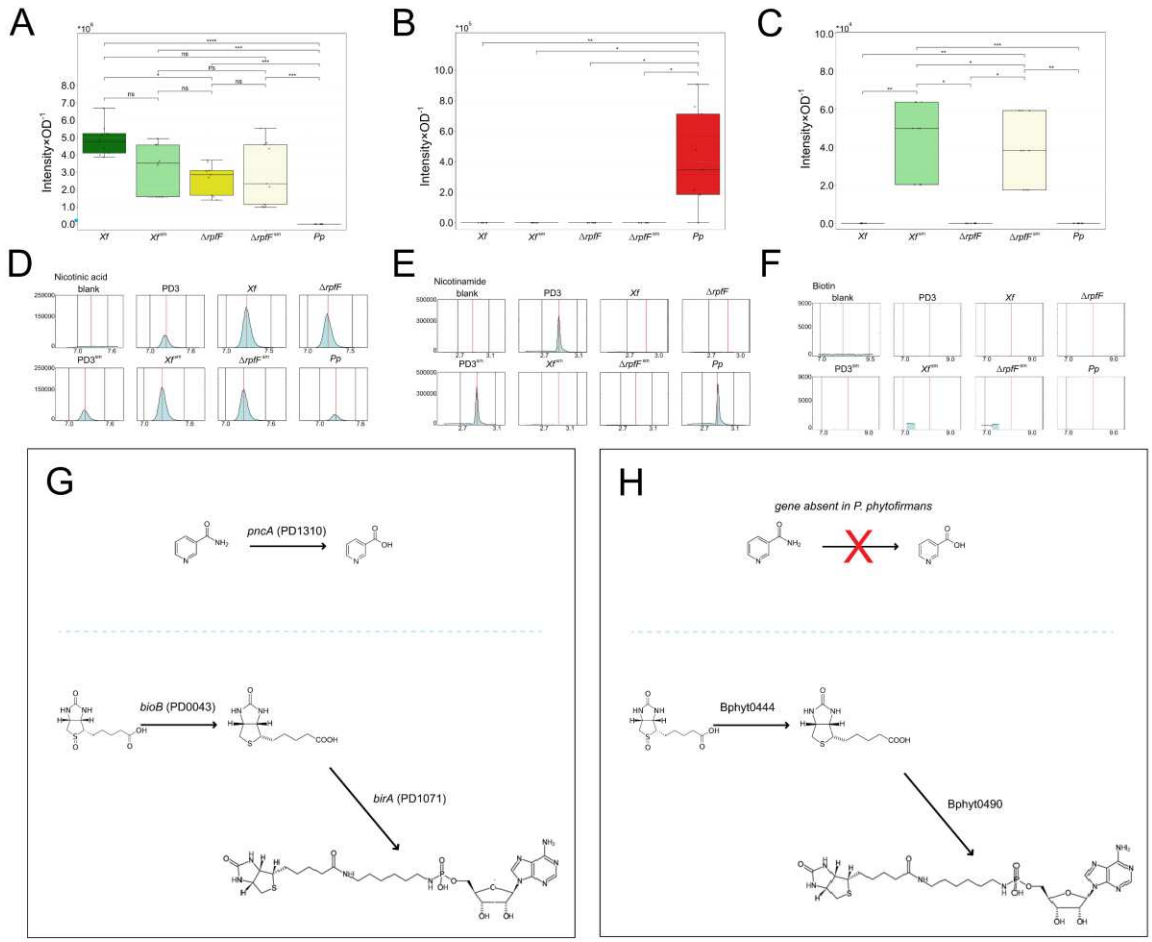

Figure 4. Vitamin B compounds expression in *Xf*, *Xf*^{sm}, Δ*rpfF*, Δ*rpfF*^{sm}, and *Pp* exometabolomes. A. Nicotinamide, B. Nicotinic acid and **C. Biotin** expression among the exometabolomes tested. Nicotinic acid is downregulated in *Xf*^{sm} to Δ*rpfF* and Δ*rpfF*^{sm} levels. Absence of the enzyme pyrazinamidase/nicotinamidase leads to Nicotinamide accumulation in *Pp* exometabolomes, there was no detection of this compound in *X. fastidiosa* strains. Biotin is detected only in *Xf*^{sm} and Δ*rpfF*^{sm} at very low levels. Significantly different expression by p-adjust value of pairwise comparison calculated by *t*-test (ns: $p > 0.05$, *: $p \leq 5.0\times10^{-2}$, **: $p \leq 5.0\times10^{-3}$, ***: $p \leq 5.0\times10^{-4}$, ****: $p \leq 5.0\times10^{-5}$). **D. Nicotinamide, E. Nicotinic acid,** and **F. Biotin EIC**. EICs of representative assessments in blank (MeOH), PD3, PD3^{sm}, *Xf*, Δ*rpfF*, *Xf*^{sm}, Δ*rpfF*^{sm}, and *Pp* extracts or exometabolomes. Main reactions in "nicotinate and nicotinamide metabolism" and in "biotin metabolism" according to KEGG pathways (www.kegg.jp/pathway/) in G. *X. fastidiosa* and H. *P. phytofirmans*, respectively.

Two Plant Hormones are Exclusively Secreted by X. fastidiosa

We conducted a comparative analysis of the levels of two compounds, 2-aminoisobutyric acid (AIB) and gibberellic acid (GA), detected within the exometabolomes of *Xf*, Δ*rpfF*, *Xf*^{sm}, Δ*rpfF*^{sm}, and *Pp*. These compounds possess implications for the interaction between *X. fastidiosa* and its plant hosts, potentially functioning as pathogen metabolite effectors. AIB, a non-proteinogenic amino acid, exists in other two isomeric forms: β-aminobutyric acid (BABA), known to induce plant disease resistance, and γ-aminobutyric acid (GABA), a neurotransmitter in animals that is also produced in plants, likely serving a signaling role. GABA was detected highly abundant in xylem sap of grapevines infected with *X. fastidiosa* . Gibberellic acid (GA), on the other hand, functions as a hormone in both plants and fungi.

Across the conditions assessed in our metabolomics analysis, AIB and GA exhibit notably similar profiles. Both compounds form three distinct clusters: (1) *Xf*, (2) *Xf*^{sm}, Δ*rpfF*, and Δ*rpfF*^{sm}, and (3) *Pp* (Figure 5A,B, Supplementary Figure S3A,B). Comparatively, AIB and GA levels prove significantly higher in *Xf* than in any other strain or treatment. *Xf*^{sm} displays reduced AIB and GA expression, akin to the observed pattern in Δ*rpfF*. Conversely, Δ*rpfF*^{sm} exhibits no significant alteration in AIB and GA expression compared to Δ*rpfF*. Notably, AIB remains undetected in the *Pp* exometabolome, while GA levels range from 6.63% to 26.89% of those detected in *Xf*, Δ*rpfF*, *Xf*^{sm}, and Δ*rpfF*^{sm} exometabolomes.

Preprints (www.preprints.org) | NOT PEER-REVIEWED | Posted: 7 December 2023 doi:10.20944/preprints202311.1985.v2

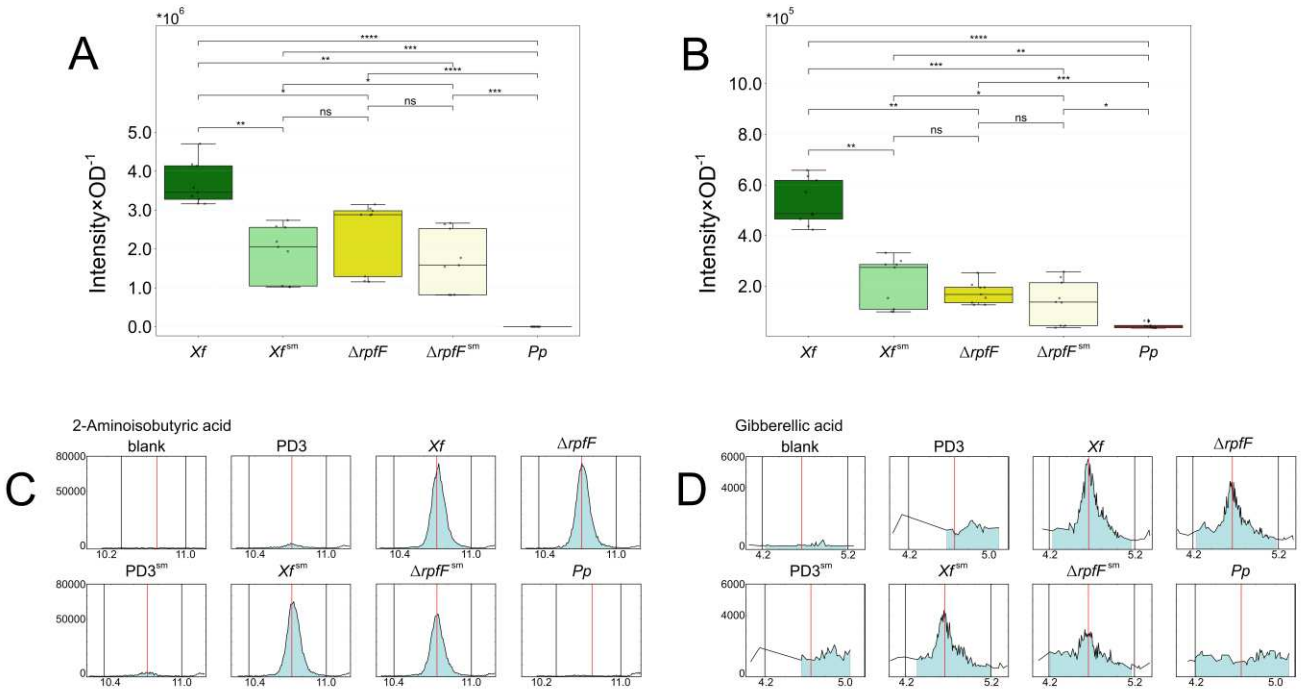

Figure 5. AIB and GA expression in *Xf*, *Xf*^{sm}, Δ*rpfF*, Δ*rpfF*^{sm}, and *Pp* exometabolomes. A. AIB and **B. GA expression.** AIB and B. GA are downregulated in *Xf*^{sm} to Δ*rpfF* and Δ*rpfF*^{sm} levels**.** Significantly different expression by p-adjust value of pairwise comparison calculated by *t*-test (ns: $p > 0.05$, *: $p \leq 5.0\times10^{-2}$, **: $p \leq 5.0\times10^{-3}$, ***: $p \leq 5.0\times10^{-4}$, ****: $p \leq 5.0\times10^{-5}$). **C. AIB** and **D. GA EICs**. EICs of representative assessments in blank (MeOH), PD3, PD3^{sm}, *Xf*, Δ*rpfF*, *Xf*^{sm}, Δ*rpfF*^{sm}, and *Pp* extracts or exometabolomes.

Chromatograms illustrate the contrast between AIB levels in *Pp*, which appear lower than those in controls, while AIB levels in *Xf* consistently remain elevated (Figure 5C). GA is generally detected at low levels across all conditions, including *Xf*. However, both *Xf* and Δ*rpfF* exhibit levels 2-to-3 times higher than controls. *Xf*^{sm} and Δ*rpfF*^{sm} exhibit increases of approximately 100% and 50%, respectively, compared to the culture medium controls. Notably, *Pp*'s GA levels mirror those of the controls (Figure 5C and D).

We investigated the potential synthesis of AIB and GA by *X. fastidiosa* or *P. phytofirmans* through the search for gene clusters for their synthesis. We examined the presence of homologous genes or clusters akin to the reported *aib* operon from *Rhodococcus wratislaviensis* [63] and the *Ga* operon from *Xanthomonas oryzae* pv *oryzicola* [9, 64]. While we identified orthologs of certain genes associated with AIB or GA synthesis (or metabolism) in *X. fastidiosa* or *P. phytofirmans*, we did not find them organized in operons as originally annotated in the genomes of *Rhodococcus wratislaviensis* and *Xanthomonas oryzae* pv *oryzicola*, respectively (Supplementary Tables S14 and S15).

Exometabolome, genome, and transcriptome integration for X. fastidiosa and P. phytofirmans

Firstly, we used NetSeed [57] — a tool for assessing metabolic network topology and determining the set of exogenously acquired compounds — to assess the metabolic networks of *X. fastidiosa* and *P. phytofirmans* predicting them as profiles in cooperation or competition. The analysis indicated a low degree of complementarity (< 0.32) and a moderate-to-high level of competition (> 0.49) between *X. fastidiosa* and *P. phytofirmans*.

In a second approach, using MAGI v.1.0 [50] we searched for a connection between annotated genes in *X. fastidiosa* or *P. phytofirmans* genomes and the detected compounds, respectively, in *Xf*, *Xf*^{sm}, Δ*rpfF*, Δ*rpfF*^{sm} or *Pp* (Tables 2, 3 and Supplementary Tables S4–S8). Out of the 121 identified compounds given as input to MAGI, 118 compounds returned results in gene-to-compound connection information from *X. fastidiosa* or *P. phytofirmans*. Specifically, all surveyed amino acids (both nEAA and EAA) exhibited connections with high reciprocity scores (≥2), i.e., compounds and annotated genes are both linked to the same reactions or metabolic pathways from the consulted databases RheA [65] or MetaCyc [66]. CDS coding for amino acid metabolism was previously annotated in the genomes of *X. fastidiosa* [27] and *P. phytofirmans* [43]. Results for AIB showed a high reciprocity score with 18 and 11 genes in *X. fastidiosa* and *P.*

Preprints (www.preprints.org) | NOT PEER-REVIEWED | Posted: 7 December 2023 doi:10.20944/preprints202311.1985.v2

phytofirmans, respectively (Supplementary Tables S4–S7). Conversely, GA displayed a notably low reciprocity score with the only two associated genes in *X. fastidiosa* (PD0286, PD0716) and likewise with the three genes (Bphyt_2421, Bphyt_2594, and Bphyt_0368) in *P. phytofirmans* (Supplementary Table S8), suggesting a limited likelihood of synthesis by these genes and, respective reactions. In *P. phytofirmans*, Bphyt_5413 is linked to nicotinamide metabolism. In *X. fastidiosa*, PD0043, PD1071, and PD1494 are linked to biotin metabolism and PD0393 and PD1310 to nicotinic acid metabolism.

Table 2. Top-scored genes-to-compounds in *X. fastidiosa* according to MAGI results.

compound name	gene id	reciprocal score	e-score reaction-to-gene	database id reaction-to-gene	e-score gene-to-reaction	database id gene-to-reaction	MAGI score
2-Aminoisobutyric acid	PD0094	2.00	200.00	ALANINE--TRNA-LIGASE-RXN	200.00	ALANINE--TRNA-LIGASE-RXN	1.58
	PD1696	2.00	200.00	RXN-16659	200.00	RXN-16659	1.58
		2.00	200.00	RXN-16649	200.00	RXN-16649	1.58
	PD1823	2.00	200.00	RHEA:20249	200.00	RHEA:20249	1.58
	PD1864	2.00	200.00	RHEA:11224	200.00	RHEA:11224	1.58
	PD1865	2.00	200.00	RHEA:23374	200.00	RHEA:23374	1.58
Alanine	PD1864	2.00	200.00	RHEA:11224	200.00	RHEA:11224	6.33
	PD1823	2.00	200.00	RHEA:20249	200.00	RHEA:20249	6.33
	PD0094	2.00	200.00	ALANINE--TRNA-LIGASE-RXN	200.00	ALANINE--TRNA-LIGASE-RXN	6.33
Arginine	PD0116	2.00	34.19	ARGININE--TRNA-LIGASE-RXN	32.31	ARGININE--TRNA-LIGASE-RXN	4.01
Asparagine	PD1947	2.00	200.00	ASPARAGINE--TRNA-LIGASE-RXN	200.00	ASPARAGINE--TRNA-LIGASE-RXN	6.33
Aspartate	PD0089	2.00	200.00	RHEA:12228	200.00	RHEA:12228	6.33
		2.00	200.00	RHEA:11375	200.00	RHEA:11375	6.33
	PD0166	2.00	200.00	RHEA:22630	200.00	RHEA:22630	6.33
	PD0291	2.00	200.00	RHEA:10932	200.00	RHEA:10932	6.33
	PD0868	2.00	200.00	RHEA:25877	200.00	RHEA:25877	6.33
	PD0946	2.00	200.00	ASPARTATE--TRNA-LIGASE-RXN	200.00	ASPARTATE--TRNA-LIGASE-RXN	6.33
	PD1273	2.00	200.00	RHEA:23777	200.00	RHEA:23777	6.33
	PD1274	2.00	200.00	RHEA:20015	200.00	RHEA:20015	6.33
	PD1627	2.00	200.00	RHEA:15753	200.00	RHEA:15753	6.33
Biotin	PD0043	2.00	140.61	2.8.1.6-RXN	145.10	2.8.1.6-RXN	5.80
	PD1071	2.00	58.42	RHEA:31118	62.94	RHEA:31118	4.66
		2.00	58.42	BIOTINLIG-RXN	62.94	BIOTINLIG-RXN	4.66
	PD1494	2.00	167.61	DETHIOBIOTIN-SYN-RXN	165.73	DETHIOBIOTIN-SYN-RXN	1.51
Cysteine	PD0655	2.00	200.00	RHEA:13285	200.00	RHEA:13285	6.33

Preprints (www.preprints.org) | NOT PEER-REVIEWED | Posted: 7 December 2023 doi:10.20944/preprints202311.1985.v2

	PD1812	2.00	156.15	RHEA:20400	154.24	RHEA:20400	5.93
	PD1841	2.00	143.27	ACSERLY-RXN	137.99	ACSERLY-RXN	5.77
	PD0118	2.00	134.13	RHEA:19398	132.24	RHEA:19398	5.71
		2.00	134.13	RHEA:25159	132.24	RHEA:25159	5.71
	PD0690	2.00	133.98	RXN0-308	132.09	RXN0-308	5.71
	PD0287	2.00	126.84	CYSTEINE--TRNA-LIGASE-RXN	124.08	CYSTEINE--TRNA-LIGASE-RXN	5.62
Gibberellic acid	PD0286	0.01	0.89	RHEA:36115	7.41	RHEA:25891	0.43
	PD0716	0.01	0.54	RHEA:36115	159.33	RHEA:13804	0.38
Nicotinic acid	PD0393	2.00	200.00	RHEA:36166	200.00	RHEA:36166	6.33
	PD1310	2.00	42.72	RHEA:14545	40.84	RHEA:14545	4.26
Glutamic acid	PD0650	2.00	200.00	RHEA:17130	200.00	RHEA:17130	6.33
	PD0654	2.00	200.00	RHEA:18052	200.00	RHEA:18052	6.33
	PD0399	2.00	200.00	RHEA:18633	200.00	RHEA:18633	6.33
	PD2062	2.00	200.00	RHEA:11613	200.00	RHEA:11613	6.33
		2.00	200.00	RHEA:15504	200.00	RHEA:15504	6.33
	PD1358	2.00	200.00	RHEA:16574	200.00	RHEA:16574	6.33
		2.00	200.00	RHEA:14329	200.00	RHEA:14329	6.33
	PD1266	2.00	200.00	RHEA:23746	200.00	RHEA:23746	6.33
	PD0089	2.00	200.00	RHEA:12228	200.00	RHEA:12228	6.33
	PD0839	2.00	200.00	RHEA:24385	200.00	RHEA:24385	6.33
	PD1447	2.00	200.00	GMP-SYN-GLUT-RXN	200.00	GMP-SYN-GLUT-RXN	6.33
	PD1848	2.00	200.00	GLURS-RXN	200.00	GLURS-RXN	6.33
	PD1026	2.00	200.00	RHEA:45804	200.00	RHEA:45804	6.33
		2.00	200.00	RHEA:16170	200.00	RHEA:16170	6.33
	PD0851	2.00	200.00	RHEA:14908	200.00	RHEA:14908	6.33
	PD0785	2.00	200.00	RHEA:15136	200.00	RHEA:15136	6.33
	PD2063	2.00	200.00	RHEA:12131	200.00	RHEA:12131	6.33
		2.00	200.00	RHEA:32192	200.00	RHEA:32192	6.33
		2.00	200.00	GLUTAMATE-SYN-THASE-FERRE-DOXIN-RXN	200.00	GLUTAMATE-SYN-THASE-FERRE-DOXIN-RXN	6.33
	PD0398	2.00	200.00	RHEA:18633	200.00	RHEA:18633	6.33
	PD0170	2.00	200.00	RHEA:21735	200.00	RHEA:21735	6.33
	PD0296	2.00	200.00	RHEA:14879	200.00	RHEA:14879	6.33
	PD0541	2.00	200.00	RHEA:15890	200.00	RHEA:15890	6.33
	PD0110	2.00	200.00	RHEA:13239	200.00	RHEA:13239	6.33
	PD0655	2.00	200.00	RHEA:13285	200.00	RHEA:13285	6.33
Glutamine	PD1447	2.00	200.00	GMP-SYN-GLUT-RXN	200.00	GMP-SYN-GLUT-RXN	6.33

 doi:10.20944/preprints202311.1985.v2

	PD0584	2.00	200.00	GLUTAMINE--TRNA-LIGASE-RXN	200.00	GLUTAMINE--TRNA-LIGASE-RXN	6.33
	PD2063	2.00	200.00	GLUTAMATE-SYN-THASE-FERRE-DOXIN-RXN	200.00	GLUTAMATE-SYN-THASE-FERRE-DOXIN-RXN	6.33
Glycine	PD1750	2.00	200.00	RHEA:15482	200.00	RHEA:15482	6.33
	PD0620	2.00	200.00	GCVMULTI-RXN	200.00	GCVMULTI-RXN	6.33
		2.00	200.00	GCVP-RXN	200.00	GCVP-RXN	6.33
	PD1810	2.00	200.00	GCVMULTI-RXN	200.00	GCVMULTI-RXN	6.33
		2.00	200.00	GCVP-RXN	200.00	GCVP-RXN	6.33
	PD0827	2.00	200.00	RHEA:17453	200.00	RHEA:17453	6.33
	PD0704	2.00	200.00	RHEA:19938	200.00	RHEA:19938	6.33
	PD0844	2.00	200.00	RHEA:13557	200.00	RHEA:13557	6.33
	PD0773	2.00	200.00	RXN0-7068	200.00	RXN0-7068	6.33
		2.00	200.00	RXN0-7082	200.00	RXN0-7082	6.33
	PD0841	2.00	170.04	GLYCINE--TRNA-LIGASE-RXN	168.01	GLYCINE--TRNA-LIGASE-RXN	6.06
	PD0840	2.00	164.75	GLYCINE--TRNA-LIGASE-RXN	162.87	GLYCINE--TRNA-LIGASE-RXN	6.02
Histidine	PD1267	2.00	200.00	RHEA:20641	200.00	RHEA:20641	6.33
	PD1772	2.00	60.65	RHEA:20641	58.79	RHEA:20641	4.66
	PD1270	2.00	26.76	HISTIDINE--TRNA-LIGASE-RXN	24.84	HISTIDINE--TRNA-LIGASE-RXN	3.76
Isoleucine	PD1437	2.00	200.00	ISOLEUCINE--TRNA-LIGASE-RXN	200.00	ISOLEUCINE--TRNA-LIGASE-RXN	6.33
Leucine	PD1230	2.00	200.00	LEUCINE--TRNA-LIGASE-RXN	200.00	LEUCINE--TRNA-LIGASE-RXN	6.33
Lysine	PD0404	2.00	200.00	LYSINE--TRNA-LIGASE-RXN	200.00	LYSINE--TRNA-LIGASE-RXN	6.33
	PD1514	2.00	69.38	RXN-1961	78.45	RXN-1961	4.86
	PD2000	2.00	55.90	RHEA:15944	53.31	RHEA:15944	1.14
Methionine	PD1590	2.00	200.00	METHIONINE--TRNA-LIGASE-RXN	200.00	METHIONINE--TRNA-LIGASE-RXN	6.33
		2.00	200.00	RXN-16165	200.00	RXN-16165	6.33
Phenylalanine	PD1911	2.00	200.00	PHENYLALANINE--TRNA-LIGASE-RXN	200.00	PHENYLALANINE--TRNA-LIGASE-RXN	6.33
	PD0665	2.00	200.00	RXN-15898	200.00	RXN-15898	1.58
Proline	PD1635	2.00	200.00	PROLINE--TRNA-LIGASE-RXN	200.00	PROLINE--TRNA-LIGASE-RXN	6.33

Preprints (www.preprints.org) | NOT PEER-REVIEWED | Posted: 7 December 2023 doi:10.20944/preprints202311.1985.v2

Serine	PD0612	2.00	200.00	RHEA:26437	200.00	RHEA:26437	6.33
		2.00	200.00	RHEA:10532	200.00	RHEA:10532	6.33
	PD1750	2.00	200.00	RHEA:15482	200.00	RHEA:15482	6.33
	PD1318	2.00	200.00	RXN0-2161	200.00	RXN0-2161	6.33
		2.00	200.00	SERINE--TRNA-LIGASE-RXN	200.00	SERINE--TRNA-LIGASE-RXN	6.33
	PD0613	2.00	200.00	RHEA:26437	200.00	RHEA:26437	6.33
		2.00	200.00	RHEA:10532	200.00	RHEA:10532	6.33
Threonine	PD1916	2.00	200.00	THREONINE--TRNA-LIGASE-RXN	200.00	THREONINE--TRNA-LIGASE-RXN	6.33
Tryptophan	PD0612	2.00	200.00	RHEA:10532	200.00	RHEA:10532	6.33
		2.00	200.00	RHEA:26437	200.00	RHEA:26437	6.33
	PD0613	2.00	200.00	RHEA:10532	200.00	RHEA:10532	6.33
		2.00	200.00	RHEA:26437	200.00	RHEA:26437	6.33
	PD1650	2.00	47.82	TRYPTOPHAN--TRNA-LIGASE-RXN	45.82	TRYPTOPHAN--TRNA-LIGASE-RXN	4.38
Tyrosine	PD0665	2.00	200.00	RXN-15898	200.00	RXN-15898	6.33
	PD0132	2.00	33.23	TYROSINE--TRNA-LIGASE-RXN	31.35	TYROSINE--TRNA-LIGASE-RXN	3.98
Valine	PD0102	2.00	200.00	VALINE--TRNA-LIGASE-RXN	200.00	VALINE--TRNA-LIGASE-RXN	6.33

Table 3. Top-scored genes-to-compounds in *P. phytofirmans* according to MAGI results.

compound name	gene id	reciprocal score	-score reaction-to-gene	database id reaction-to-gene	e-score gene-to-reaction	database id gene-to-reaction	MAGI score
Cysteine	phyt_3930	2.00	200.00	RHEA:13285	200.00	RHEA:13285	6.33
	phyt_4072	2.00	200.00	RXN-17172	200.00	RXN-17172	6.33
		2.00	200.00	RXN-15881	200.00	RXN-15881	6.33
	Bphyt_2579	2.00	200.00	RXN0-308	200.00	RXN0-308	6.33
	phyt_3068	2.00	200.00	RHEA:28784	200.00	RHEA:28784	6.33
	phyt_0110	2.00	200.00	RHEA:13285	200.00	RHEA:13285	6.33
	phyt_3953	2.00	200.00	RHEA:13285	200.00	RHEA:13285	6.33
	phyt_2579	2.00	177.70	RXN-14385	175.79	RXN-14385	6.13
	phyt_2510	2.00	175.50	CYSTEINE--TRNA-LIGASE-RXN	171.77	YSTEINE--TRNA-LIGASE-RXN	6.10
Gibberellic acid	Bphyt_5231	0.01	18.39	RXN-14318	39.82	RXN-16827	0.23
		0.01	18.39	RXN-14317	39.82	RXN-16827	0.23
		0.01	18.39	RXN-7617	39.82	RXN-16827	0.23
Nicotinamide	phyt_5413	2.00	200.00	RHEA:16150	200.00	RHEA:16150	6.33

Next, the resulting genes from MAGI analysis as described above were used for functional annotation via gene ontology [67,68], through OmicsBox (Supplementary Tables S9–S13). From all the annotated functions, we focused on

Preprints (www.preprints.org) | NOT PEER-REVIEWED | Posted: 7 December 2023 doi:10.20944/preprints202311.1985.v2

the top five over-enriched and top 5 under-enriched functions (Figure 6A). Despite minor variations in Δ*rpfF*, *Xf*^{sm}, and Δ*rpfF*^{sm}—especially when compared to *Xf*—over-represented functions generally appeared common across those conditions, such as "ligase activity, forming carbon-nitrogen bonds," "oxidoreductase activity, acting on NAD(P)H," and "ligase activity" ($log_2FC > 5$). Functions like "Vitamin B6 binding," "pyridoxal phosphate binding," and "tricarboxylic acid cycle" were enriched in *Xf*, Δ*rpfF*, *Xf*^{sm}, and Δ*rpfF*^{sm}, but under-enriched in *Pp*. Conversely, "CoA-ligase activity" and "fatty acid ligase activity" were highly over-represented in *Pp* ($log_2FC > 5$), whereas they were not enriched in *Xf*, Δ*rpfF*, *Xf*^{sm}, or Δ*rpfF*^{sm} (Figure 6A).

Preprints (www.preprints.org) | NOT PEER-REVIEWED | Posted: 7 December 2023 doi:10.20944/preprints202311.1985.v2

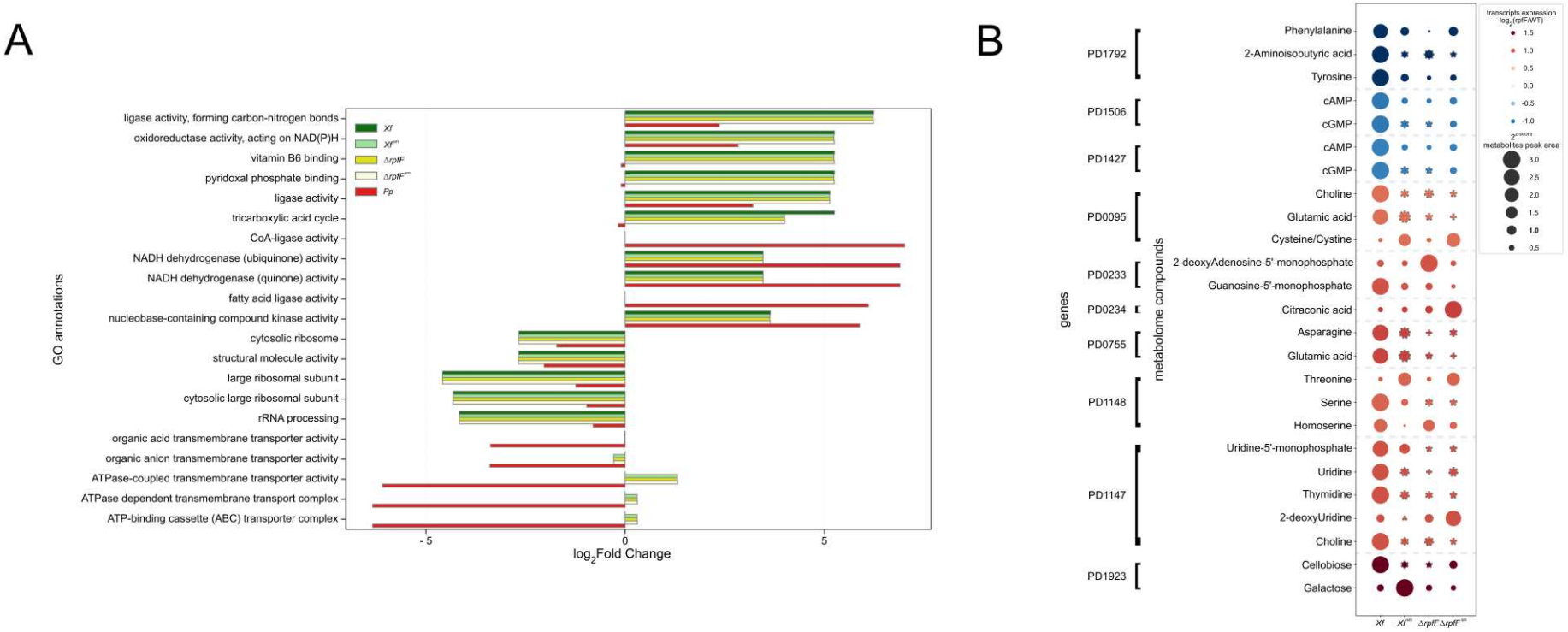

Figure 6. Integration of metabolomics data with functional genomics and RpfF regulon (transcriptomic). A. GO Enrichment Analysis performed with genes retrieved from MAGI analysis. GO Annotations displayed are the top 5 over- and underrepresented in the 5 conditions tested, all the showed GO Annotations passed the p-value adjusted < 0.05 criteria. **B. Public data from RpfF Regulon was crossed with genes predicted to be directly involved with the synthesis of the compounds detected in the exometabolomes.** Color code, blue-to-red, indicates down and up-regulated genes in the RpfF Regulon. The shape size of circles indicates the expression level in peak size of compounds detected among the conditions tested. Peak size numbers were normalized into squared z-scores in order to maximize expression level differences among conditions. Dark gray dashed-circles around dots or "bubbles" indicate DEM in relation to *Xf*.

Preprints (www.preprints.org) | NOT PEER-REVIEWED | Posted: 7 December 2023 doi:10.20944/preprints202311.1985.v2

Finally, we lined up our metabolome data with a previously published RpfF-Regulon, i.e., transcriptomic data obtained with microarray technology [3]. We did not directly and statistically integrate metabolome and transcriptome data, but, instead, we tracked genes directly linked to the detected compounds (obtained from MAGI) and cross-referenced them with the published differentially expressed genes (DEGs) in the RpfF-Regulon (Figure 6B). A consistent pattern exists where genes downregulated in the Δ*rpfF* strain were associated with lower levels of metabolites detected in Δ*rpfF* compared to *Xf*, including 2-Aminoisobutyric acid, cAMP, cGMP, Phenylalanine, and Tyrosine. In contrast, the upregulated DEGs in the Δ*rpfF* strain showed no pattern at the metabolite level. Instead, metabolite expression within *Xf*^{sm}, Δ*rpfF*, and Δ*rpfF*^{sm} differed when compared to *Xf*, signifying a lack of regularity but rather an upregulation of specific metabolites in these conditions. Metabolites cross-checked as upregulated in metabolome and as a consequence of upregulated genes in RpfF-regulon include Choline, Cysteine, 2-deoxyAdenosine-5′-monophosphate, Guanosine-5′-monophosphate, Citraconic acid, Asparagine, Glutamic acid, Threonine, Serine, Homoserine, Uridine-5′-monophosphate, Uridine, Thymidine, 2-deoxyUridine, Cellobiose, and Galactose.

4. Discussion

In prior studies, it was demonstrated that the co-inoculation of *P. phytofirmans* along with *X. fastidiosa* leads to a reduction in the symptoms of leaf scorching induced by *X. fastidiosa* in grapevines. This ameliorative effect was attributed to the activation of plant defense genes, specifically involving pathways related to salicylic acid and ethylene [33]. It was further reported that the topical application of *P. phytofirmans* with a surfactant, was efficient and sufficient for PD control in grapevines, even though the protection was spatially limited [34].

In our investigation, we observe that the cultivation of *X. fastidiosa* in PD3 medium supplemented with 20% spent media from *P. phytofirmans* (*Xf*^{sm} and Δ*rpfF*^{sm}) results in a perturbation of the *X. fastidiosa* biofilm structure. In particular, the biofilm exhibits an increased volume and extends across the air-liquid media interface, deviating from the usual compacted ring pattern observed in the liquid culture of *Xf*. Additionally, Baccari and colleagues [33] previously highlighted a synergistic impact arising from the concurrent infection of *X. fastidiosa* and *P. phytofirmans*, leading to the activation of plant defense mechanisms. However, in that work, there was no exploration of a direct interaction between *P. phytofirmans* and *X. fastidiosa*, at the metabolomic level, that could provide insights into their relevance for conventional virulence and plant colonization.

While comparing metabolite profiles, we found a considerable disparity in the number of identified metabolites in *Pp* in comparison to *Xf*, *Xf*^{sm}, Δ*rpfF*, and Δ*rpfF*^{sm}. The limited abundance of detected metabolites in *Pp*, coupled with reduced variability among replicates, contributes to its distinct distribution pattern observed in the Principal Coordinate Analysis (PCoA). While replicates of the *Xf* exometabolome exhibit close clustering, there is noticeable variability within the *Xf*^{sm}, Δ*rpfF*, and Δ*rpfF*^{sm} exometabolomes, although statistical analyses such as Permdisp and Permanova confirm significance across all conditions. The absence of a functional quorum sensing (QS) system in the Δ*rpfF* strain is mirrored in its altered metabolite expression profile, akin to findings in other omics analyses such as transcriptomics and outer membrane vesicle (OMV) proteome [3,69]. Notably, the exometabolome profile of *Xf*^{sm} shows greater similarity to that of Δ*rpfF* as opposed to *Xf*. Nevertheless, Δ*rpfF*^{sm} exometabolomes maintain an overall likeness to Δ*rpfF*. Consequently, we report that *Pp* affects *Xf*^{sm} exometabolome, although this effect is notably diminished in the impaired DSF-producing strain (Δ*rpfF*^{sm}).

X. fastidiosa is known to exhibit a hypersecretory trait, particularly regarding virulence proteins and extracellular vesicles (EVs), as established in prior reports [23,24,69,70]. Expanding on this, our study targeted the characterization of *X. fastidiosa* exometabolome, focusing on low molecular weight compounds. Our findings indicate that, in overall comparison among the 5 different groups, *Xf* has a higher expression of compounds. Pairwise comparison of *Xf* versus *Xf*^{sm}, Δ*rpfF*, Δ*rpfF*^{sm}, or *Pp* shows a similar pattern, with, at least 80% of compounds being upregulated in *Xf*. It remains an area for further investigation to determine whether the quorum sensing system interferes with the ability of *X. fastidiosa* to secrete metabolites. The high secretion of certain metabolites, as will be discussed below, could benefit *X. fastidiosa* from the plant defense mechanisms as the phytopathogen is still not established in a higher population under the influence of the QS system [2].

Another point to highlight, Δ*rpfF*^{sm} exometabolome suggests a less responsive profile to *P. phytofirmans* spent media than *Xf*^{sm}. Detected metabolite levels in Δ*rpfF*/Δ*rpfF*^{sm} are more similar to the levels in *Xf*/*Xf*^{sm} (e.g., they had 114 compounds detected in common, from which only 2 were DEM downregulated in Δ*rpfF*/Δ*rpfF*^{sm}). Taken together, these observations indicate that at least partially, the detected responses to *P. phytofirmans* occur by disturbance of DSF signaling in *Xf*. Here we were limited to metabolites being detected through the LCMS method in a HILIC column. Other coupled MS analyses could complement our findings, e.g., using a c18 column (focused on non-polar and large

compounds) or through a surface-based MS technique such as NIMS, which would increase the detected metabolites as seen for other models [71,72].

From the exometabolomes of *Xf*, *Xf*^{sm}, Δ*rpfF*, Δ*rpfF*^{sm}, and *Pp*, two sets of compounds were further studied: amino acids (EAA and nEAA), vitamin B complex, and hormones. The average GLN:GLU ratios are highly similar in *Xf* and Δ*rpfF* (0.52 and 0.57, respectively). These values are regarded in the literature as (> 0.5) indicative of N-replete cells [62]. The average GLN:GLU ratios in *Xf*^{sm} and Δ*rpfF*^{sm} show an increased trend from treatments without contact with *P. phytofirmans* spent media, although without statistical significance. Secondly, the EAA and nEAA overall levels were inspected using their chromatogram abundance profiles. EAA are more abundant than nEAA in *Xf* when compared to *Xf*^{sm}. It is noteworthy that a high ratio of EAA:nEAA was reported in the bacteriomes of four xylem-feeding insects [10]. We speculate that *X. fastidiosa* exometabolomes showing especially high EAA might be an indication of attractiveness to insect vectors. Indeed, studies in the field that had simultaneously evaluated the xylem of host plants and insects report that adults chose plants with high amino acid concentrations [19]. The levels of EAA and nEAA are significantly different between *Xf* and Δ*rpfF*. Another point, a study conducted by Daugherty and colleagues [73] indicated that the insect prefers plants with lower symptoms than plants with disease symptoms. In fact, the Δ*rpfF* mutant reaches faster a systemic infection in grapevines compared to the WT strain and Δ*rpfF* has a lower fitness for being less transmitted by the insect vector when compared to the WT strain. Moreover, Δ*rpfF* has a restricted ability to form cell aggregates, which is the successful state of *X. fastidiosa* when acquired by the insect vector feeding on xylem sap, as reported for WT strain [41]. In this case, it remains to be tested whether the lower level of amino acids secreted by the Δ*rpfF* would add to its worse tendency to be acquired by the insect. *P. phytofirmans* had very low or totally absent detection of amino acids in its exometabolome under the conditions here tested. Nevertheless, *P. phytofirmans* has all the predicted pathways for amino acid production according to its genome annotation [43].

Similar to amino acids, compounds within the Vitamin B complex hold particular significance for insect-borne phytopathogens [74]. Our metabolomics analysis unveiled the presence of nicotinamide, nicotinic acid, and biotin. Notably, the interplay between nicotinamide and nicotinic acid mirrors the pattern of coding sequences present or absent in *X. fastidiosa* and *P. phytofirmans*. The enzyme nicotinamidase is predicted to convert the compound nicotinamide into nicotinic acid (both being isoforms of B3 vitamin). In fact, in *X. fastidiosa* genome is predicted the enzyme *pncA* (nicotinamidase) is, whereas *P. phytofirmans* genome there is no homolog of a nicotinamidase gene predicted. This conversion was indeed corroborated by our metabolomics analysis (Figure 3, Supplementary Figure S4). Symbiont bacteria, e.g., *Wolbachia* and *Baumannia*, have been reported to convert precursors and provide B vitamins to their insect xylem-sap feeding hosts [74]. Nevertheless, vitamin B3 is usually not among the B vitamins this symbiont bacteria are able to yield. It remains to be further investigated if the *X. fastidiosa* provision of this specific isoform of B vitamin increases the host plant attractiveness towards the insect vector. We also detected biotin, another compound from vitamin B, in *Xf*^{sm} and Δ*rpfF*^{sm}. Nevertheless, there was a low level of expression in both exometabolomes and a low level of identification.

AIB is reported as the immediate precursor of ethylene in higher plants. Specifically, AIB inhibits ethylene production because it acts through competitive inhibition of the conversion of 1-aminocyclopropane-1-carboxylic acid to ethylene [75]. Very little is known about AIB metabolism in bacteria, although it is reported that the AIB catabolism in *Rhodococcus wratislaviensis* C31-06 leads to its conversion into α-methyl-D-serine, and after other downstream metabolic conversions, it results in pyruvic acid [63]. In turn, gibberellic acid is a well-known plant growth promoter [76]. In bacteria, it seems the role of gibberellins is linked to pathogenicity, where secreted gibberellins could act as virulence factors, most probably by suppressing jasmonic acid formation and, ultimately, impairing the host defense response [64], as reported in the rice pathogen *Xanthomonas oryzae* pv. *oryzicola* [77].

The identity of compounds AIB and GA was confirmed by comparing with standards by MS. Nevertheless, operons for AIB and GA synthesis are absent in *X. fastidiosa* and *P. phytofirmans* as seen in other bacteria, it remains to be further investigated which genes are directly linked with their synthesis in *X. fastidiosa* or *P. phytofirmans*. As mentioned before, GABA was highly detected in the xylem sap of grapevines infected with *X. fastidiosa* [15]. Also, the fact that is well established that these hormones have a function on plant growth and development makes it even more interesting to address the role of AIB and GA as virulence factors for *X. fastidiosa* during disease progression. AIB and GA do not seem to have a synergistic effect therefore it remains unclear how their concomitant secretion would benefit *X. fastidiosa*. AIB has a higher expression than GA (3,444,408.4 intensity×OD^{-1} versus 506,103.7 intensity×OD^{-1}, respectively) and in case its function prevails it would most probably induce an impairment of host plant growth and *X. fastidiosa* could take advantage of that by a slower response from the host plant in its vasculature system. The identification and characterization of changes in specialized metabolites caused by *X. fastidiosa* in plant hosts are still in the early stages. However, collectively, these findings present a promising outlook on the reprogramming of metabolism following the interaction

of plants with the phytopathogen [78]. For instance, in infected Leccino plants, higher amounts of salicylic acid was observed compared to Cellina di Nardò plants. Leccino variety develops milder symptoms compared to those observed on the Cellina di Nardò variety [79]. Although it has been described a GA cluster in *Burkholderia* species [80], a closely related species, such a gene cluster was not found in the *P. phytofirmans* genome (Supplementary Figure S4).

Reverse ecology analysis revealed generally low complementarity (< 0.32) and medium-to-high competition scores (> 0.49) for *X. fastidiosa* towards *P. phytofirmans* and vice-versa as stated in the results section. Therefore, *X. fastidiosa* and *P. phytofirmans* are predicted competitive bacterial species. This has implications for the search for a microorganism that can act as a biocontrol for the diseases caused by *X. fastidiosa,* as seen in the natural occurrence of other endophytes, e.g., *M. mesophilicum* in orange trees [81].

Overrepresented Gene Ontology (GO) annotations reveal distinctions not only between *Xf* and *Pp* but also with *Xf* ^{sm}, Δ*rpfF*, and Δ*rpfF*^{sm}. Collectively, these findings suggest that *P. phytofirmans* induces a metabolic perturbation in *Xf*^{sm}, rendering it more similar to Δ*rpfF*. This observation is further supported by the overall similarity between Δ*rpfF*^{sm} and Δ*rpfF*. The specific metabolite or set of metabolites produced by *P. phytofirmans*, which is not the subject of investigation in this study and appears not to be synthesized by a Δ*rpfF* ortholog (as reported by Baccari and colleagues [33]), may still be exerting a disruptive effect on quorum sensing. Notably, quorum sensing disruption appears to be an effective strategy for disease suppression. For instance, in a study both tobacco, a model host, and orange tree, a natural host, that produces DSF have shown increased resistance to *X. fastidiosa*. The disruption in signaling confounds bacterial behavior and hinders disease development [82].

Overall, we demonstrated that metabolomics can be used for the prospection of *X. fastidiosa* footprint. The secretion of EAA and nEAA, vitamin B complex, and the ratio between Gln:Glu are influenced by *P. phytofirmans* spent media and also, by the absence of a functional QS signaling. Finally, metabolites with plant metabolism and growth properties, AIB and GA, were detected, which are down-regulated in *X. fastidiosa* when in contact with *P. phytofirmans* spent media or in the absence of QS signaling. To our knowledge, this is the first report of its exometabolome in response to another endophyte.

Supplementary Materials: The following supporting information can be downloaded at the website of this paper posted on Preprints.org, Figure S1: List of EICs from Essential Amino Acids and Non Essential Amino Acids in all conditions and replicates; Figure S2: List of EICs from Nicotinic Acid, Nicotinamide and Biotin in all conditions and replicates; Figure S3: List of EICs from Isoaminobutyric Acid and Gibberellic Acid in all conditions and replicates; Figure S4: Comparison between *Burkholderia cepacia* genome to its close related species, *P. phytofirmans*; Table S1: Summary of metabolites standard comparison; Table S2: List of metabolites with presence-absence detection analysis; Table S3: Final list of confirmed metabolites and pairwise statistical analysis; Table S4: MAGI *Xf*'s genome-metabolome integration; Table S5: MAGI *Xf* ^{sm}' genome-metabolome integration; Table S6: MAGI Δ*rpfF*'s genome-metabolome integration; Table S7: MAGI Δ*rpfF*^{sm}' genome-metabolome integration; Table S8: MAGI *Pp*'s genome-metabolome integration; Table S9: *Xf*'s genome-metabolome extracted gene ontology enrichment; Table S10: *Xf*^{sm}' genome-metabolome extracted gene ontology enrichment; Table S11: Δ*rpfF*'s genome-metabolome extracted gene ontology enrichment; Table S12: Δ*rpfF*^{sm}' genome-metabolome extracted gene ontology enrichment; Table S13: *Pp*'s genome-metabolome extracted gene ontology enrichment; Table S14: AIB operon *Rhodococcus wratislaviensis* and relative homologous genes in *X. fastidiosa* and *P. phytofirmans*; Table S15: GA operon in *Xanthomonas oryzae* pv *oryzicola* and relative homologous genes in *X. fastidiosa* and *P. phytofirmans*.

Author Contributions: Conceptualization: A.M.d.S., A.L., O.R.F.-J. Methodology: O.R.F.-J, A.L., D.B., J.M-J, S.M.K., C.B., B.P.B. Computing resources: D.B., J.M-J, B.P.B. Data curation: O.R.F.-J, A.L., D.B., J.M-J, S.M.K., B.P.B. Formal analysis: O.R.F.-J., A.L., P.A.Z., S.K., B.P.B. Visualization: O.R.F.-J, P.A.Z, A.M.d.S. Writing—original draft preparation: O.R.F.-J., P.A.Z. Writing—review and editing: O.R.F.-J, P.A.Z, A.M.d.S. Supervision: A.M.d.S, T.R.N., S.E.L. Funding acquisition: A.M.d.S, T.R.N., and S.E.L. All authors read, provided critical review, and approved the final manuscript. All authors have read and agreed to the published version of the manuscript.

Funding: This research was partially funded by São Paulo Research Foundation (FAPESP), grant number 08/11703-4, and by Coordination for the Improvement of Higher Education Personnel (CAPES), by the Program Sandwich-Doctorate Abroad (PDSE), grant number 99999.009713/2014-00. D.B. received a fellowship from CAPES (88887.285065/2018-00 and 88887.318125/2019-00). A.M.d.S. received a research fellowship award 309182/2016-6 from the National Council for Scientific and Technological Development (CNPq). A.L and S.M.K were supported by the Office of Science, Office of Biological and Environmental Research, of the US Department of Energy, Award No. DE-SC0012627. T.R.N. and B.P.B. were partially supported by the former award and the U.S. Department of Energy Joint Genome Institute (https://ror.org/04xm1d337), a DOE Office of Science User Facility, is supported by the Office of Science of the U.S. Department of Energy operated under Contract No. DE-AC02-05CH11231.

Data Availability Statement: *X. fastidiosa* and *P. phytofirmans* genomic sequences were accessed from the GenBank RefSeq database at NCBI (National Center for Biotechnology Information).

Conflicts of Interest: The authors declare no conflict of interest. The funders had no role in the design of the study; in the collection, analyses, or interpretation of data; in the writing of the manuscript, or in the decision to publish the results.

References

1. Sicard, A.; Zeilinger, A. R.; Vanhove, M.; Schartel, T. E.; Beal, D. J.; Daugherty, M. P.; Almeida, R. P. P., Xylella fastidiosa: Insights into an Emerging Plant Pathogen. *Annual Review of Phytopathology, Vol 56* **2018,** 56, 181-202.
2. Chatterjee, S.; Almeida, R. P.; Lindow, S., Living in two worlds: the plant and insect lifestyles of *Xylella fastidiosa*. *Annu Rev Phytopathol* **2008,** 46, 243-71.
3. Wang, N.; Li, J. L.; Lindow, S. E., RpfF-dependent regulon of Xylella fastidiosa. *Phytopathology* **2012,** 102, (11), 1045-53.
4. Ionescu, M.; Yokota, K.; Antonova, E.; Garcia, A.; Beaulieu, E.; Hayes, T.; Iavarone, A. T.; Lindow, S. E., Promiscuous Diffusible Signal Factor Production and Responsiveness of the Xylella fastidiosa Rpf System. *MBio* **2016,** 7, (4).
5. Roper, C.; Castro, C.; Ingel, B., Xylella fastidiosa: bacterial parasitism with hallmarks of commensalism. *Curr Opin Plant Biol* **2019,** 50, 140-147.
6. Rapicavoli, J.; Ingel, B.; Blanco-Ulate, B.; Cantu, D.; Roper, C., Xylella fastidiosa: an examination of a re-emerging plant pathogen. *Mol Plant Pathol* **2018,** 19, (4), 786-800.
7. Morris, C. E.; Moury, B., Revisiting the Concept of Host Range of Plant Pathogens. *Annual Review of Phytopathology, Vol 57, 2019* **2019,** 57, 63-90.
8. Parniske, M., Uptake of bacteria into living plant cells, the unifying and distinct feature of the nitrogen-fixing root nodule symbiosis. *Curr Opin Plant Biol* **2018,** 44, 164-174.
9. Nagel, R.; Turrini, P. C.; Nett, R. S.; Leach, J. E.; Verdier, V.; Van Sluys, M. A.; Peters, R. J., An operon for production of bioactive gibberellin A(4) phytohormone with wide distribution in the bacterial rice leaf streak pathogen Xanthomonas oryzae pv. oryzicola. *New Phytol* **2017,** 214, (3), 1260-1266.
10. Ankrah, N. Y. D.; Wilkes, R. A.; Zhang, F. Q.; Aristilde, L.; Douglas, A. E., The Metabolome of Associations between Xylem-Feeding Insects and their Bacterial Symbionts. *Journal of Chemical Ecology* **2020,** 46, (8), 735-744.
11. Yang, J.; Masoudi, A.; Li, H.; Gu, Y.; Wang, C.; Wang, M.; Yu, Z.; Liu, J., Microbial community structure and niche differentiation under different health statuses of Pinus bungeana in the Xiong'an New Area in China. *Front Microbiol* **2022,** 13, 913349.
12. De Silva, N. I.; Brooks, S.; Lumyong, S.; Hyde, K. D., Use of endophytes as biocontrol agents. *Fungal Biol Rev* **2019,** 33, (2), 133-148.
13. Saldanha, L. L.; Allard, P. M.; Dilarri, G.; Codesido, S.; Gonzalez-Ruiz, V.; Queiroz, E. F.; Ferreira, H.; Wolfender, J. L., Metabolomic- and Molecular Networking-Based Exploration of the Chemical Responses Induced in Citrus sinensis Leaves Inoculated with Xanthomonas citri. *J Agr Food Chem* **2022**.
14. Ryffel, F.; Helfrich, E. J. N.; Kiefer, P.; Peyriga, L.; Portais, J. C.; Piel, J.; Vorholt, J. A., Metabolic footprint of epiphytic bacteria on Arabidopsis thaliana leaves. *Isme J* **2016,** 10, (3), 632-643.
15. Zaini, P. A.; Nascimento, R.; Gouran, H.; Cantu, D.; Chakraborty, S.; Phu, M.; Goulart, L. R.; Dandekar, A. M., Molecular Profiling of Pierce's Disease Outlines the Response Circuitry of Vitis vinifera to Xylella fastidiosa Infection. *Front Plant Sci* **2018,** 9, 771.
16. Chen, X. L.; Sun, M. C.; Chong, S. L.; Si, J. P.; Wu, L. S., Transcriptomic and Metabolomic Approaches Deepen Our Knowledge of Plant-Endophyte Interactions. *Frontiers in Plant Science* **2022,** 12.
17. Cariddi, C.; Saponari, M.; Boscia, D.; De Stradis, A.; Loconsole, G.; Nigro, F.; Porcelli, F.; Potere, O.; Martelli, G. P., Isolation of a *Xylella fastidiosa* strain infecting olive and oleander in Apulia, Italy. *J Plant Pathol* **2014,** 96, (2), 425-429.
18. Desprez-Loustau, M.-L.; Balci, Y.; Cornara, D.; Gonthier, P.; Robin, C.; Jacques, M.-A., Is Xylella fastidiosa a serious threat to European forests? *Forestry: An International Journal of Forest Research* **2020,** 94, (1), 1-17.
19. Krugner, R.; Sisterson, M. S.; Backus, E. A.; Burbank, L. P.; Redak, R. A., Sharpshooters: a review of what moves Xylella fastidiosa. *Austral Entomol* **2019,** 58, (2), 248-267.
20. Saponari, M.; Loconsole, G.; Cornara, D.; Yokomi, R. K.; De Stradis, A.; Boscia, D.; Bosco, D.; Martelli, G. P.; Krugner, R.; Porcelli, F., Infectivity and transmission of Xylellua fastidiosa by Philaenus spumarius (Hemiptera: Aphrophoridae) in Apulia, Italy. *J Econ Entomol* **2014,** 107, (4), 1316-9.
21. Huang, W. J.; Reyes-Caldas, P.; Mann, M.; Seifbarghi, S.; Kahn, A.; Almeida, R. P. P.; Béven, L.; Heck, M.; Hogenhout, S. A.; Coaker, G., Bacterial Vector-Borne Plant Diseases: Unanswered Questions and Future Directions. *Molecular Plant* **2020,** 13, (10), 1379-1393.
22. Roper, M. C.; Greve, L. C.; Warren, J. G.; Labavitch, J. M.; Kirkpatrick, B. C., *Xylella fastidiosa* requires polygalacturonase for colonization and pathogenicity in *Vitis vinifera* grapevines. *Molecular Plant-Microbe Interactions* **2007,** 20, (4), 411-419.
23. Nascimento, R.; Gouran, H.; Chakraborty, S.; Gillespie, H. W.; Almeida-Souza, H. O.; Tu, A.; Rao, B. J.; Feldstein, P. A.; Bruening, G.; Goulart, L. R.; Dandekar, A. M., The Type II Secreted Lipase/Esterase LesA is a Key Virulence Factor Required for Xylella fastidiosa Pathogenesis in Grapevines (vol 6, 18598, 2016). *Sci Rep-Uk* **2016,** 6.
24. Feitosa, O. R.; Stefanello, E.; Zaini, P. A.; Nascimento, R.; Pierry, P. M.; Dandekar, A. M.; Lindow, S. E.; da Silva, A. M., Proteomic and Metabolomic Analyses of Xylella fastidiosa OMV-Enriched Fractions Reveal Association with Virulence Factors and Signaling Molecules of the DSF Family. *Phytopathology* **2019,** 109, (8), 1344-1353.
25. Block, A.; Li, G. Y.; Fu, Z. Q.; Alfano, J. R., Phytopathogen type III effector weaponry and their plant targets. *Current Opinion in Plant Biology* **2008,** 11, (4), 396-403.

26. Kvitko, B. H.; Collmer, A., Discovery of the Hrp Type III Secretion System in Phytopathogenic Bacteria: How Investigation of Hypersensitive Cell Death in Plants Led to a Novel Protein Injector System and a World of Inter-Organismal Molecular Interactions Within Plant Cells. *Phytopathology* **2023**.
27. Van Sluys, M. A.; Monteiro-Vitorello, C. B.; Camargo, L. E.; Menck, C. F.; Da Silva, A. C.; Ferro, J. A.; Oliveira, M. C.; Setubal, J. C.; Kitajima, J. P.; Simpson, A. J., Comparative genomic analysis of plant-associated bacteria. *Annu Rev Phytopathol* **2002,** 40, 169-89.
28. De La Fuente, L.; Merfa, M. V.; Cobine, P. A.; Coleman, J. J., Pathogen Adaptation to the Xylem Environment. *Annu Rev Phytopathol* **2022,** 60, 163-186.
29. Sawana, A.; Adeolu, M.; Gupta, R. S., Molecular signatures and phylogenomic analysis of the genus Burkholderia: proposal for division of this genus into the emended genus Burkholderia containing pathogenic organisms and a new genus Paraburkholderia gen. nov. harboring environmental species. *Front Genet* **2014,** 5, 429.
30. Sessitsch, A.; Coenye, T.; Sturz, A. V.; Vandamme, P.; Barka, E. A.; Salles, J. F.; Van Elsas, J. D.; Faure, D.; Reiter, B.; Glick, B. R.; Wang-Pruski, G.; Nowak, J., Burkholderia phytofirmans sp. nov., a novel plant-associated bacterium with plant-beneficial properties. *International journal of systematic and evolutionary microbiology* **2005,** 55, 1187-1192.
31. Mitter, B.; Petric, A.; Shin, M. W.; Chain, P. S.; Hauberg-Lotte, L.; Reinhold-Hurek, B.; Nowak, J.; Sessitsch, A., Comparative genome analysis of Burkholderia phytofirmans PsJN reveals a wide spectrum of endophytic lifestyles based on interaction strategies with host plants. *Front Plant Sci* **2013,** 4, 120.
32. Miotto-Vilanova, L.; Jacquard, C.; Courteaux, B.; Wortham, L.; Michel, J.; Clement, C.; Barka, E. A.; Sanchez, L., Burkholderia phytofirmans PsJN Confers Grapevine Resistance against Botrytis cinerea via a Direct Antimicrobial Effect Combined with a Better Resource Mobilization. *Front Plant Sci* **2016,** 7, 1236.
33. Baccari, C.; Antonova, E.; Lindow, S., Biological Control of Pierce's Disease of Grape by an Endophytic Bacterium. *Phytopathology* **2019,** 109, (2), 248-256.
34. Lindow, S.; Koutsoukis, R.; Meyer, K. M.; Baccari, C., Control of Pierce's disease of grape with Paraburkholderia phytofirmans PsJN in the field. *Phytopathology* **2023**.
35. Sue, T.; Obolonkin, V.; Griffiths, H.; Villas-Boas, S. G., An Exometabolomics Approach to Monitoring Microbial Contamination in Microalgal Fermentation Processes by Using Metabolic Footprint Analysis. *Appl Environ Microb* **2011,** 77, (21), 7605-7610.
36. Drenos, F., Mechanistic insights from combining genomics with metabolomics. *Curr Opin Lipidol* **2017,** 28, (2), 99-103.
37. Liu, R.; Bao, Z. X.; Zhao, P. J.; Li, G. H., Advances in the Study of Metabolomics and Metabolites in Some Species Interactions. *Molecules* **2021,** 26, (11).
38. Villas-Boas, S. G.; Noel, S.; Lane, G. A.; Attwood, G.; Cookson, A., Extracellular metabolomics: a metabolic footprinting approach to assess fiber degradation in complex media. *Analytical biochemistry* **2006,** 349, (2), 297-305.
39. Villas-Boas, S. G.; Mas, S.; Akesson, M.; Smedsgaard, J.; Nielsen, J., Mass spectrometry in metabolome analysis. *Mass Spectrom Rev* **2005,** 24, (5), 613-46.
40. Newman, K. L.; Almeida, R. P.; Purcell, A. H.; Lindow, S. E., Use of a green fluorescent strain for analysis of *Xylella fastidiosa* colonization of *Vitis vinifera*. *Appl Environ Microbiol* **2003,** 69, (12), 7319-27.
41. Newman, K. L.; Almeida, R. P. P.; Purcell, A. H.; Lindow, S. E., Cell-cell signaling controls Xylella fastidiosa interactions with both insects and plants. *Proceedings of the National Academy of Sciences of the United States of America* **2004,** 101, (6), 1737-1742.
42. Frommel, M. I.; Nowak, J.; Lazarovits, G., Growth Enhancement and Developmental Modifications of in Vitro Grown Potato (Solanum tuberosum spp. tuberosum) as Affected by a Nonfluorescent Pseudomonas sp. *Plant Physiol* **1991,** 96, (3), 928-36.
43. Weilharter, A.; Mitter, B.; Shin, M. V.; Chain, P. S. G.; Nowak, J.; Sessitsch, A., Complete Genome Sequence of the Plant Growth-Promoting Endophyte Burkholderia phytofirmans Strain PsJN. *J Bacteriol* **2011,** 193, (13), 3383-3384.
44. King, E. O.; Ward, M. K.; Raney, D. E., Two simple media for the demonstration of pyocyanin and fluorescin. *J Lab Clin Med* **1954,** 44, (2), 301-7.
45. Zaini, P. A.; De La Fuente, L.; Hoch, H. C.; Burr, T. J., Grapevine xylem sap enhances biofilm development by Xylella fastidiosa. *FEMS microbiology letters* **2009,** 295, (1), 129-134.
46. Bowen, B. P.; Northen, T. R., Dealing with the unknown: metabolomics and metabolite atlases. *J Am Soc Mass Spectrom* **2010,** 21, (9), 1471-6.
47. Yao, Y.; Sun, T.; Wang, T.; Ruebel, O.; Northen, T.; Bowen, B. P., Analysis of Metabolomics Datasets with High-Performance Computing and Metabolite Atlases. *Metabolites* **2015,** 5, (3), 431-42.
48. Sumner, L. W.; Amberg, A.; Barrett, D.; Beale, M. H.; Beger, R.; Daykin, C. A.; Fan, T. W. M.; Fiehn, O.; Goodacre, R.; Griffin, J. L.; Hankemeier, T.; Hardy, N.; Harnly, J.; Higashi, R.; Kopka, J.; Lane, A. N.; Lindon, J. C.; Marriott, P.; Nicholls, A. W.; Reily, M. D.; Thaden, J. J.; Viant, M. R., Proposed minimum reporting standards for chemical analysis. *Metabolomics* **2007,** 3, (3), 211-221.
49. Gower, J. C., Some Distance Properties of Latent Root and Vector Methods Used in Multivariate Analysis. *Biometrika* **1966,** 53, 325-&.
50. Erbilgin, O.; Rubel, O.; Louie, K. B.; Trinh, M.; Raad, M.; Wildish, T.; Udwary, D.; Hoover, C.; Deutsch, S.; Northen, T. R.; Bowen, B. P., MAGI: A Method for Metabolite Annotation and Gene Integration. *ACS Chem Biol* **2019,** 14, (4), 704-714.
51. Merkel, D., Docker: lightweight linux containers for consistent development and deployment. *Linux journal* **2014,** 2014, 2.
52. Gotz, S.; Garcia-Gomez, J. M.; Terol, J.; Williams, T. D.; Nagaraj, S. H.; Nueda, M. J.; Robles, M.; Talon, M.; Dopazo, J.; Conesa, A., High-throughput functional annotation and data mining with the Blast2GO suite. *Nucleic Acids Res* **2008,** 36, (10), 3420-3435.

53. Grigoriev, I. V.; Nordberg, H.; Shabalov, I.; Aerts, A.; Cantor, M.; Goodstein, D.; Kuo, A.; Minovitsky, S.; Nikitin, R.; Ohm, R. A.; Otillar, R.; Poliakov, A.; Ratnere, I.; Riley, R.; Smirnova, T.; Rokhsar, D.; Dubchak, I., The genome portal of the Department of Energy Joint Genome Institute. *Nucleic Acids Res* **2012,** 40, (Database issue), D26-32.
54. Delcher, A. L.; Phillippy, A.; Carlton, J.; Salzberg, S. L., Fast algorithms for large-scale genome alignment and comparison. *Nucleic Acids Res* **2002,** 30, (11), 2478-2483.
55. Michelini, S.; Balakrishnan, B.; Parolo, S.; Matone, A.; Mullaney, J. A.; Young, W.; Gasser, O.; Wall, C.; Priami, C.; Lombardo, R.; Kussmann, M., A reverse metabolic approach to weaning: in silico identification of immune-beneficial infant gut bacteria, mining their metabolism for prebiotic feeds and sourcing these feeds in the natural product space. *Microbiome* **2018,** 6, (1), 171.
56. Levy, R.; Borenstein, E., Reverse Ecology: from systems to environments and back. *Adv Exp Med Biol* **2012,** 751, 329-45.
57. Carr, R.; Borenstein, E., NetSeed: a network-based reverse-ecology tool for calculating the metabolic interface of an organism with its environment. *Bioinformatics* **2012,** 28, (5), 734-5.
58. Levy, R.; Borenstein, E., Metabolic modeling of species interaction in the human microbiome elucidates community-level assembly rules. *Proc Natl Acad Sci U S A* **2013,** 110, (31), 12804-9.
59. Kreimer, A.; Doron-Faigenboim, A.; Borenstein, E.; Freilich, S., NetCmpt: a network-based tool for calculating the metabolic competition between bacterial species. *Bioinformatics* **2012,** 28, (16), 2195-7.
60. Kim, S.; Chen, J.; Cheng, T. J.; Gindulyte, A.; He, J.; He, S. Q.; Li, Q. L.; Shoemaker, B. A.; Thiessen, P. A.; Yu, B.; Zaslavsky, L.; Zhang, J.; Bolton, E. E., PubChem 2023 update. *Nucleic Acids Res* **2022**.
61. Bennett, G. M.; Moran, N. A., Heritable symbiosis: The advantages and perils of an evolutionary rabbit hole. *Proc Natl Acad Sci U S A* **2015,** 112, (33), 10169-76.
62. Flynn, K. J.; Dickson, D. M. J.; Al-Amoudi, O. A., The ratio of glutamine:glutamate in microalgae: a biomarker for N-status suitable for use at natural cell densities. *Journal of Plankton Research* **1989,** 11, (1), 165-170.
63. Hibi, M.; Fukuda, D.; Kenchu, C.; Nojiri, M.; Hara, R.; Takeuchi, M.; Aburaya, S.; Aoki, W.; Mizutani, K.; Yasohara, Y.; Ueda, M.; Mikami, B.; Takahashi, S.; Ogawa, J., A three-component monooxygenase from Rhodococcus wratislaviensis may expand industrial applications of bacterial enzymes. *Commun Biol* **2021,** 4, (1).
64. Salazar-Cerezo, S.; Martinez-Montiel, N.; Garcia-Sanchez, J.; Perez, Y. T. R.; Martinez-Contreras, R. D., Gibberellin biosynthesis and metabolism: A convergent route for plants, fungi and bacteria. *Microbiol Res* **2018,** 208, 85-98.
65. Bansal, P.; Morgat, A.; Axelsen, K. B.; Muthukrishnan, V.; Coudert, E.; Aimo, L.; Hyka-Nouspikel, N.; Gasteiger, E.; Kerhornou, A.; Neto, T. B.; Pozzato, M.; Blatter, M. C.; Ignatchenko, A.; Redaschi, N.; Bridge, A., Rhea, the reaction knowledgebase in 2022. *Nucleic Acids Res* **2022,** 50, (D1), D693-D700.
66. Caspi, R.; Billington, R.; Keseler, I. M.; Kothari, A.; Krummenacker, M.; Midford, P. E.; Ong, W. K.; Paley, S.; Subhraveti, P.; Karp, P. D., The MetaCyc database of metabolic pathways and enzymes - a 2019 update. *Nucleic Acids Res* **2020,** 48, (D1), D445-D453.
67. Ashburner, M.; Ball, C. A.; Blake, J. A.; Botstein, D.; Butler, H.; Cherry, J. M.; Davis, A. P.; Dolinski, K.; Dwight, S. S.; Eppig, J. T.; Harris, M. A.; Hill, D. P.; Issel-Tarver, L.; Kasarskis, A.; Lewis, S.; Matese, J. C.; Richardson, J. E.; Ringwald, M.; Rubin, G. M.; Sherlock, G.; Consortium, G. O., Gene Ontology: tool for the unification of biology. *Nat Genet* **2000,** 25, (1), 25-29.
68. Gene Ontology, C.; Aleksander, S. A.; Balhoff, J.; Carbon, S.; Cherry, J. M.; Drabkin, H. J.; Ebert, D.; Feuermann, M.; Gaudet, P.; Harris, N. L.; Hill, D. P.; Lee, R.; Mi, H.; Moxon, S.; Mungall, C. J.; Muruganugan, A.; Mushayahama, T.; Sternberg, P. W.; Thomas, P. D.; Van Auken, K.; Ramsey, J.; Siegele, D. A.; Chisholm, R. L.; Fey, P.; Aspromonte, M. C.; Nugnes, M. V.; Quaglia, F.; Tosatto, S.; Giglio, M.; Nadendla, S.; Antonazzo, G.; Attrill, H.; Dos Santos, G.; Marygold, S.; Strelets, V.; Tabone, C. J.; Thurmond, J.; Zhou, P.; Ahmed, S. H.; Asanitthong, P.; Luna Buitrago, D.; Erdol, M. N.; Gage, M. C.; Ali Kadhum, M.; Li, K. Y. C.; Long, M.; Michalak, A.; Pesala, A.; Pritazahra, A.; Saverimuttu, S. C. C.; Su, R.; Thurlow, K. E.; Lovering, R. C.; Logie, C.; Oliferenko, S.; Blake, J.; Christie, K.; Corbani, L.; Dolan, M. E.; Drabkin, H. J.; Hill, D. P.; Ni, L.; Sitnikov, D.; Smith, C.; Cuzick, A.; Seager, J.; Cooper, L.; Elser, J.; Jaiswal, P.; Gupta, P.; Jaiswal, P.; Naithani, S.; Lera-Ramirez, M.; Rutherford, K.; Wood, V.; De Pons, J. L.; Dwinell, M. R.; Hayman, G. T.; Kaldunski, M. L.; Kwitek, A. E.; Laulederkind, S. J. F.; Tutaj, M. A.; Vedi, M.; Wang, S. J.; D'Eustachio, P.; Aimo, L.; Axelsen, K.; Bridge, A.; Hyka-Nouspikel, N.; Morgat, A.; Aleksander, S. A.; Cherry, J. M.; Engel, S. R.; Karra, K.; Miyasato, S. R.; Nash, R. S.; Skrzypek, M. S.; Weng, S.; Wong, E. D.; Bakker, E.; Berardini, T. Z.; Reiser, L.; Auchincloss, A.; Axelsen, K.; Argoud-Puy, G.; Blatter, M. C.; Boutet, E.; Breuza, L.; Bridge, A.; Casals-Casas, C.; Coudert, E.; Estreicher, A.; Livia Famiglietti, M.; Feuermann, M.; Gos, A.; Gruaz-Gumowski, N.; Hulo, C.; Hyka-Nouspikel, N.; Jungo, F.; Le Mercier, P.; Lieberherr, D.; Masson, P.; Morgat, A.; Pedruzzi, I.; Pourcel, L.; Poux, S.; Rivoire, C.; Sundaram, S.; Bateman, A.; Bowler-Barnett, E.; Bye, A. J. H.; Denny, P.; Ignatchenko, A.; Ishtiaq, R.; Lock, A.; Lussi, Y.; Magrane, M.; Martin, M. J.; Orchard, S.; Raposo, P.; Speretta, E.; Tyagi, N.; Warner, K.; Zaru, R.; Diehl, A. D.; Lee, R.; Chan, J.; Diamantakis, S.; Raciti, D.; Zarowiecki, M.; Fisher, M.; James-Zorn, C.; Ponferrada, V.; Zorn, A.; Ramachandran, S.; Ruzicka, L.; Westerfield, M., The Gene Ontology knowledgebase in 2023. *Genetics* **2023,** 224, (1).
69. Ionescu, M.; Zaini, P. A.; Baccari, C.; Tran, S.; da Silva, A. M.; Lindow, S. E., Xylella fastidiosa outer membrane vesicles modulate plant colonization by blocking attachment to surfaces. *Proceedings of the National Academy of Sciences of the United States of America* **2014,** 111, (37), E3910-8.
70. Smolka, M. B.; Martins, D.; Winck, F. V.; Santoro, C. E.; Castellari, R. R.; Ferrari, F.; Brum, I. J.; Galembeck, E.; Coletta, H. D.; Machado, M. A.; Marangoni, S.; Novello, J. C., Proteome analysis of the plant pathogen *Xylella fastidiosa* reveals major cellular and extracellular proteins and a peculiar codon bias distribution. *Proteomics* **2003,** 3, (2), 224-237.
71. Jacoby, R. P.; Martyn, A.; Kopriva, S., Exometabolomic Profiling of Bacterial Strains as Cultivated Using Arabidopsis Root Extract as the Sole Carbon Source. *Molecular Plant-Microbe Interactions* **2018,** 31, (8), 803-813.

72. Louie, K. B.; Bowen, B. P.; Cheng, X.; Berleman, J. E.; Chakraborty, R.; Deutschbauer, A.; Arkin, A.; Northen, T. R., "Replica-extraction-transfer" nanostructure-initiator mass spectrometry imaging of acoustically printed bacteria. *Anal Chem* **2013,** 85, (22), 10856-62.
73. Daugherty, M. P.; Rashed, A.; Almeida, R. P. P.; Perring, T. M., Vector preference for hosts differing in infection status: sharpshooter movement and Xylella fastidiosa transmission. *Ecol Entomol* **2011,** 36, (5), 654-662.
74. Douglas, A. E., The B vitamin nutrition of insects: the contributions of diet, microbiome and horizontally acquired genes. *Curr Opin Insect Sci* **2017,** 23, 65-69.
75. Wang, H.; Zhi, W.; Qu, H.; Lin, H.; Jiang, Y., Application of alpha-aminoisobutyric acid and beta-aminoisobutyric acid inhibits pericarp browning of harvested longan fruit. *Chem Cent J* **2015,** 9, (1), 54.
76. Phinney, B. O., Growth Response of Single-Gene Dwarf Mutants in Maize to Gibberellic Acid. *Proceedings of the National Academy of Sciences of the United States of America* **1956,** 42, (4), 185-189.
77. Lu, X.; Hershey, D. M.; Wang, L.; Bogdanove, A. J.; Peters, R. J., An ent-kaurene-derived diterpenoid virulence factor from Xanthomonas oryzae pv. oryzicola. *New Phytologist* **2015,** 206, (1), 295-302.
78. Vergine, M.; Nicolì, F.; Sabella, E.; Aprile, A.; De Bellis, L.; Luvisi, A., Secondary Metabolites in Plant Interaction. *Pathogens* **2020,** 9, (9).
79. Novelli, S.; Gismondi, A.; Di Marco, G.; Canuti, L.; Nanni, V.; Canini, A., Plant defense factors involved in Olea europaea resistance against Xylella fastidiosa infection. *J Plant Res* **2019,** 132, (3), 439-455.
80. Joo, G. J.; Kang, S. M.; Hamayun, M.; Kim, S. K.; Na, C. I.; Shin, D. H.; Lee, I. J., Burkholderia sp KCTC 11096BP as a newly isolated gibberellin producing bacterium. *Journal of Microbiology* **2009,** 47, (2), 167-171.
81. Azevedo, J. L.; Araujo, W. L.; Lacava, P. T., The diversity of citrus endophytic bacteria and their interactions with Xylella fastidiosa and host plants. *Genetics and Molecular Biology* **2016,** 39, (4), 476-491.
82. Caserta, R.; Souza-Neto, R. R.; Takita, M. A.; Lindow, S.; Souza, A., Ectopic expression of Xylella fastidiosa rpfF conferring production of diffusible signal factor in transgenic tobacco and citrus alters pathogen behavior and reduces disease severity. *Molecular plant-microbe interactions : MPMI* **2017**.